MICROCOPY RESOLUTION TEST CHART
NATIONAL BUREAU OF STANDARDS-1963-A

Washington
HINGTON·UNIVERSITY·IN·ST·LOUIS

AD-A184 165
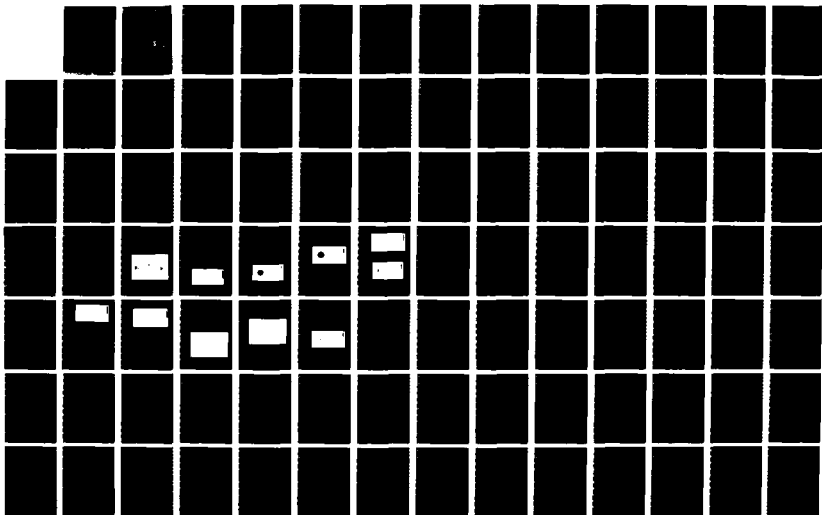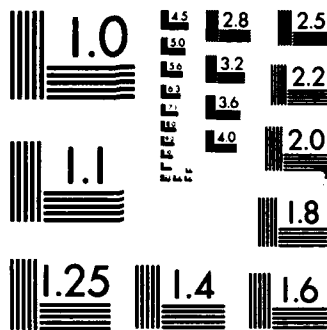
DELAY-DOPPLER RADAR IMAGING

Semi-Annual Progress Report No. 2
O.N.R. Contract N00014-86-K-0370
Period: 1 December 1986 - 30 May 1987

ELECTRONIC SYSTEMS
AND SIGNALS
RESEARCH LABORATORY

Department of Electrical Engineering
Campus Box 1127
One Brookings Drive
Washington University

Principal Investigator: Donald L. Snyder

87 8 4 005

DELAY-DOPPLER IMAGING-RADAR

Semi-Annual Progress Report No. 2

Office of Naval Research Contract Number N00014-86-K-0370

Period Covered: 1 December 1986 - 30 May 1987

Principal Investigator:

Donald L. Snyder
Director, Electronic Systems and Signals Research Laboratory
Washington University
Campus Box 1127
One Brookings Drive
St. Louis, Missouri 63130

Scientific Program Director:

Dr. Rabinder Madan
Office of Naval Research
Code 1114SE
800 North Quincy Street
Arlington, Virginia 22217-5000

DISTRIBUTION

<u>copies</u>

Mr. John W. Michalski   1
Office of Naval Research
Resident Representative
Federal Building, Room 286
536 South Clark Street
Chicago, Illinois 60605-1588

Dr. Rabinder N. Madan   1
Office of Naval Research
800 N. Quincy Street
Code 1114SE
Arlington, VA 22217-5000

Director   1
Naval Research Laboratory
Attn: Code 2627
Washington, DC 20375

Defense Technical Information Center   12
Building 5
Cameron Station
Alexandria, VA 22314

Mr. Harper J. Whitehouse   1
Naval Ocean Systems Center
Code 7402
San Diego, California 92152

Table of Contents

1. Introduction

This second semi-annual progress report contains a summary of work accomplished on O.N.R. contract number N00014-86-K-0370, Delay-Doppler Radar-Imaging, during the period from 1 December 1986 to 30 May 1987.

The goal of this project is to formulate and investigate new approaches for forming images of radar targets from spotlight-mode, delay-doppler measurements. These measurements could be acquired with a high-resolution radar-imaging system operating with an optical or radio frequency carrier. Two approaches are under study. The first is motivated by an image-reconstruction algorithm used in radionuclide imaging called the "confidence-weighted" algorithm. The second is one based on more fundamental principles which starts with a mathematical model that accurately describes the physics of an imaging radar-system and then uses statistical-estimation theory with this model to derive processing algorithms.

Spotlight-mode high-resolution radar-imaging relies upon the relative motion between the transmitter, target, and receiver. The target is illuminated by a series of transmitted pulses. The return for each pulse is a superposition of reflections from various locations on the target, with each location affecting the pulse by introducing both a delay and a doppler shift. The returns are processed to produce an image of the target.

The common approach is to use the same transmitted pulse for each illumination of the target. The returns are processed using a two-dimensional Fourier transform to produce the target's image in delay/doppler or range/cross-range coordinates [1,2]. Our goal is to compare images produced in this standard way with those produced using the alternative approaches we are developing.

Bernfeld [3] appears to be the first to introduce the idea for radar imaging of modifying the pulse shape on successive illuminations of the target. We are using Bernfeld's idea in the confidence-weighted approach. With this, the FM chirp rate of each pulse is varied so that the angles made by the ambiguity functions in the delay/doppler plane are caused to vary over the full range of angles between 0° and 180°. Use is then made of the fact that, on the average, the output of a receiver consisting of filters matched to doppler shifted versions of a transmitted pulse is the two-dimensional convolution of ambiguity function of the pulse with the scattering

function of the target [4], an output we call the delay/doppler power function. Given the delay/doppler power functions for each illumination, the target's ambiguity function can be determined using the confidence-weighted algorithm [5].

2. Summary of Work Accomplished

During this reporting period, Mr. Robert C. Lewis completed the implementation of conventional, two-dimensional Fourier-transform processing for use in comparison studies with the new algorithms we are developing. This work is documented in his M.S. thesis [6], which is included here in Appendix 4.1. A computer simulation was developed of inverse synthetic-aperture radar processing using a stepped-frequency transmitted waveform. This simulation was validated by the generation of several images from target scattering functions. A mathematical model for a slowly fluctuating point target in the presence of additive noise was applied to simulating the received signal from an extended diffuse target. This model was implemented in the computer simulation. The effects on conventional radar-images of the quantitatively specified noise are given. Images of simple radar targets were produced for a random reflectivity process having varying degrees of coherence time. The results show that random variations in the reflectivity have a significant effect on the quality of conventional ISAR images. The target is unrecognizable unless the reflectivity has a long coherence time compared to the duration of the radar illumination.

We are currently performing a similar simulation in which the confidence-weighted approach is used to produce the images. The results will be presented in the next progress report. A preliminary observation is that the images produced this way appear to be less degraded by random temporal variations in the reflectivity.

The use of the two-dimensional Fourier transform to produce target images is based on a deterministic model for the radar-reflection data. However, commonly accepted models for returns from diffuse targets at optical and radio frequencies is not deterministic. We anticipate that improved target images will be obtained by taking the random nature of the radar return into account during the processing. For this reason, we have initiated work in formulating the high-resolution radar-imaging problem as a problem in statistical estimation. Our first results have been prepared as a report [7], which is included here in Appendix 4.2. This report is presently being revised for publication in the IEEE Trans. on Information Theory, with the

main objective in the revision being to reduce the dimensionality of the matrices required to form the image. The main result of this report is an iterative algorithm for producing target images.

3. References

1. D. L. Mensa, *High Resolution Radar Imaging*, Artech House, Dedham, MA, 1981.

2. D. R. Wehner, *High Resolution Radar*, Artech House, Dedham, MA, 1987.

3. M. Bernfied, "CHIRP Doppler Radar," Proc. IEEE, Vol. 72, pp. 540-541, April 1984.

4. D. L. Snyder, H. J. Whitehouse, J. T. Wohlschlaeger, and R. C. Lewis, "A New Approach to Radar/Sonar Imaging," Proc. 1986 SPIE Conference on Advanced Algorithms and Architectures, Vol. 696, pp. 134-139, 1986.

5. D. L. Snyder, L. J. Thomas, Jr., and M. M. Ter-Pogossian, "A Mathematical Model for Positron Emission Tomography Systems Having Time-of-Flight Measurements," IEEE Trans. on Nuclear Science, Vol. NS-28, pp. 3575-3583, June 1981.

6. R. C. Lewis, "Inverse Synthetic-Aperture Radar Imaging," M.S. Thesis, Sever Institute of Technology, Washington University, May 1987. See Appendix 4.1.

7. D. L. Snyder, J. A. O'Sullivan, and M. I. Miller, "The Use of Maximum-Likelihood Estimation for Forming Images of Diffuse Radar-Targets from Delay-Doppler Data," Tech. Rpt. Electronic Systems and Signals Research Laboratory, Washington University, St. Louis, May 1987. See Appendix 4.2.

4. Appendices

4.1 Copy of Reference 6.

R. C. Lewis, "Inverse Synthetic-Aperture Radar Imaging," M.S. Thesis, Sever Institute of Technology, Washington University, May 1987.

WASHINGTON UNIVERSITY

SEVER INSTITUTE OF TECHNOLOGY

INVERSE SYNTHETIC-APERTURE RADAR IMAGING

by

Robert C. Lewis

Prepared under the direction of Dr. Donald L. Snyder

A thesis presented to the Sever Institute of
Washington University in partial fulfillment
of the requirements for the degree of

MASTER OF SCIENCE

May 1987

Saint Louis, Missouri

WASHINGTON UNIVERSITY
SEVER INSTITUTE OF TECHNOLOGY

ABSTRACT

INVERSE SYNTHETIC-APERTURE RADAR IMAGING

by Robert C. Lewis

ADVISOR: Professor D. L. Snyder

May 1987

Saint Louis, Missouri

A computer simulation was developed of inverse synthetic-aperture radar processing using a stepped-frequency transmitted waveform. This simulation is validated by the generation of several images from target scattering functions. A mathematical model for a slowly fluctuating point target in the presence of additive noise is applied to simulating the received signal from an extended diffuse target. This model is implemented in the computer simulation. The effects on radar images of the quantitatively specified noise are presented.

iii

Table of Contents

List of Figures

List of Figures (Continued)

INVERSE SYNTHETIC-APERTURE RADAR IMAGING

1. INTRODUCTION

Inverse synthetic-aperture radar (ISAR) imaging is a technique for making two-dimensional delay-doppler images of flying aircraft at long distances. The resulting image is a spatial distribution of the reflected signal power from the surface of the target at sufficient resolution to distinguish features for recognition. These radar images are often judged similar enough to visual images to enable feature recognition and target identification.

There are many other applications in which the ISAR imaging techniques are used. Sensors using other frequencies and signal media are used; for example, underwater sound (SONAR) is used in submarines to make images of other ships. Also, the idea of forming an image of an unknown target for recognition purposes is not the only objective. Radar images are made in laboratories to resolve the radar cross section of features on an aircraft or other radar reflector.

This thesis addresses the application of airborne imaging of a target aircraft. It documents the results of a project during which a computer program was developed to generate an ISAR image from a speci-fied target scattering function. The results of this development are demonstrated by examples of images which were generated. In addition, a

noise model was developed for radar data and was implemented in the simulation to provide a quantitative analysis tool useful for observing the effects of random reflectivity and additive channel noise on radar images. Resulting images are presented.

1.1 BACKGROUND

The research for this thesis was conducted as a part of a radar imaging project in the newly formed Electronic Systems and Signals Research Laboratory of the Electrical Engineering department at Washington University. It contributes to the laboratory's objective of developing an ISAR processing capability to be used as an aid in studying the performance of conventional ISAR imaging compared to new imaging algorithms currently in development, see (1)[*]. The new algorithms are based on different approaches to the radar imaging problem, and their relative performance to ISAR is a major laboratory interest.

1.2 RADAR IMAGING

The signal transmitted by a radar can be designed so that received echo signals can be measured to yield information about the appearance of the target. The measurements are usually displayed as a two-dimensional image, like a photograph. A well-known experience which is an analogy to this operation is using a flashlight in a dark room to illuminate an object within the light beam. The flashlight is analogous

---

[*] The numbers in parentheses in the text indicate references in the Bibliography.

to the radar illuminating the target. A radar illuminates a target with microwave energy instead of light. The eye can resolve the illuminated surface of an object quite finely so that detailed features are seen. Likewise the radar processing must finely resolve the surface of the illuminated target. An image shows the variation of reflected power across the surface of the object to the spatial resolution limit. The radar's target also resides within the beam width of illumination. One important difference of radar imaging, compared with visual imaging, is that the target must be rotating.

The radar-signal processing must make use of two received signal parameters in order to produce an image. The parameters must be directly related to separate orthogonal components of the two-dimensional position across the object as projected on the image plane. In radar imaging, the received signal parameters used are round-trip delay and doppler frequency shift. Any point on the surface of the target can be located in a delay-doppler two-dimensional image plane. To understand this, refer to the geometry of the location of the radar set relative to the target, as shown in Figure 1.1. A narrow pulse transmitted from the radar and reflected from a point target will be received after a round-trip delay time. The delay locates the point in down-range position. A large target is a rigid body rotating about an axis at its geometric center, and points distributed on its surface are moving at different velocities, depending on each one's distance from the axis. For a group of points with the same delay location, contained in a slice of the target at a down-range position, their cross-range position corresponds to distance from the axis of rotation, and therefore velocity. A target point's velocity causes a doppler frequency

shift of the reflected radar signal. By measuring doppler frequency, a point target can thus be located in cross-range by using doppler. The delay-doppler plane indicated in Figure 1.1 corresponds directly to the x-y position plane shown.
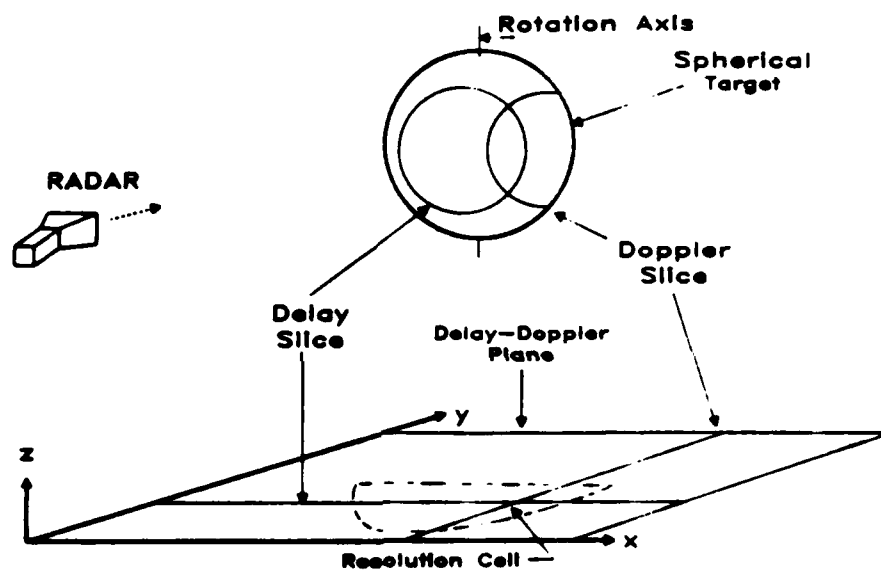
Figure 1.1 ISAR Imaging Geometry

1.3 ISAR IMAGING

The relative rotation between the radar and the target may come from either the radar being fixed while the target rotates, or equivalently, the radar rotates about the fixed target. The latter situation is used in synthetic aperture radar (SAR) imaging where a ground map is made as an aircraft flies by. The descriptive term "synthetic aperture" refers to the equivalent antenna aperture derived from

integrating received signals over a long flight path. A longer antenna results in finer resolution of the target, thus a long flight path while imaging is desirable. Ground mapping by SAR techniques preceded the use of ISAR, or inverse SAR, for aircraft-to-aircraft imaging. The description "inverse" refers to using a fixed radar and a rotating target, which is close to the actual situation in air-to-air imaging when using the radar's aircraft as a position reference. The computer processing used in the above two cases of imaging are nearly the same.

The ISAR imaging geometry is shown in Figure 1.1. The axis of rotation is normal to the line between the radar and the center of the target. The resulting image shows the point of view of looking along the axis of rotation, with illumination coming from the side.

A large target's body rotation axis may have arbitrary angle of intersection with the radar line of sight. As described by Wehner in(3), in this case the "effective rotation axis" is coplanar with the radar line of sight and the true rotation axis and perpendicular to the radar line of sight. The effective rotation vector has magnitude of the vector projection of the true rotation vector. Also, the delay-doppler image plane is normal to the effective rotation axis.

2. ISAR TECHNIQUES AND WAVEFORMS

This chapter contains a description of two implementations of ISAR processing. They differ in the waveforms transmitted. The first uses a linear-FM pulse waveform. The second uses a stepped-frequency pulse-burst waveform. The second waveform is a discretization of the linear-FM pulse waveform. It is best described in comparison to the linear-FM pulse, and so both techniques are described below to allow a better overall view of ISAR techniques.

2.1 LINEAR-FM ISAR IMAGING

The technique of using a linear-FM pulse waveform for ISAR imaging is described in (2). A series of pulses is transmitted to produce an image. Each pulse has a rectangular envelope and linear swept frequency during the pulse. The instantaneous frequency of a linear-FM pulse is illustrated in Figure 2.1.
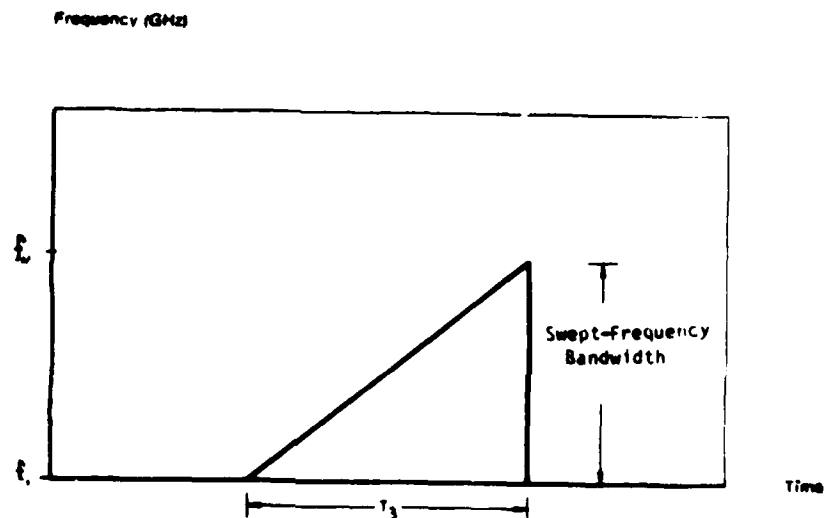
Frequency (GHz)

The Instantaneous Frequency of a Linear-FM Pulse

Figure 2.1

The received signal is processed in the following way. It is mixed with the transmitted signal and sampled, to produce a discrete time signal which when Fourier transformed will yield the range profile of the target. An illustration of the radar system components along with a comparison of the transmitted and received signals for a point target and the mixer output is shown in Figure 2.2. The mixer output signal is sampled and the discrete Fourier transform (DFT) is calculated to get a sequence of complex numbers. The magnitude values of this complex number sequence would be the target range profile, but in getting an ISAR image several linear-FM pulses are transmitted and received, mixed, sampled and transformed. The complex range profiles resulting from each pulse are aligned in rows of a two-dimensional array so the columns represent a range bin, the same range value. This two-dimensional array corresponds to the image plane shown in Figure 1.1 such that the rows, each containing a mixer output sequence resulting from a pulse, are aligned parallel to the y-axis. The columns are parallel to the x-axis.
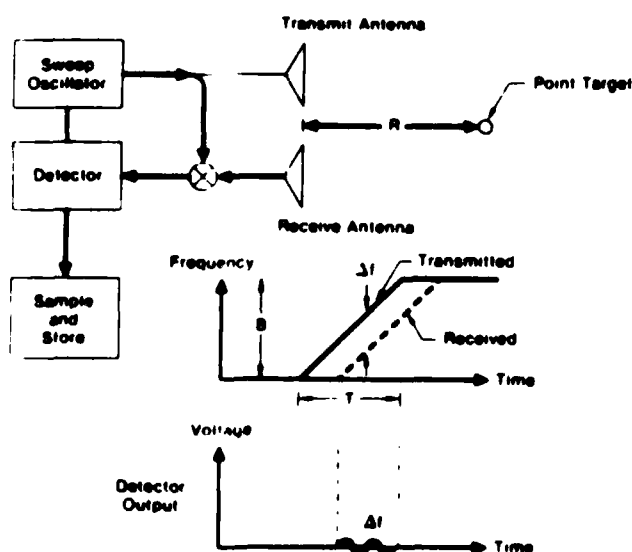
Figure 2.2. The Linear-FM Imaging Systems and Waveforms

The DFT of each column in the array is then calculated. This sorts the doppler frequencies of the data in the range bins yielding cross-range profiles when the magnitudes of the resulting complex numbers are calculated. After this second step, the array contains an image which shows the distribution of reflected energy over the surface of the target.

2.2 STEPPED-FREQUENCY ISAR IMAGING

This variation on ISAR techniques, from (3), may be described as using a discretized version of the linear-FM pulse waveform. The stepped-frequency waveform consists of a sequence of narrow pulses, with rectangular envelopes, comprising a burst of pulses. This burst of pulses is illustrated in Figure 2.3.
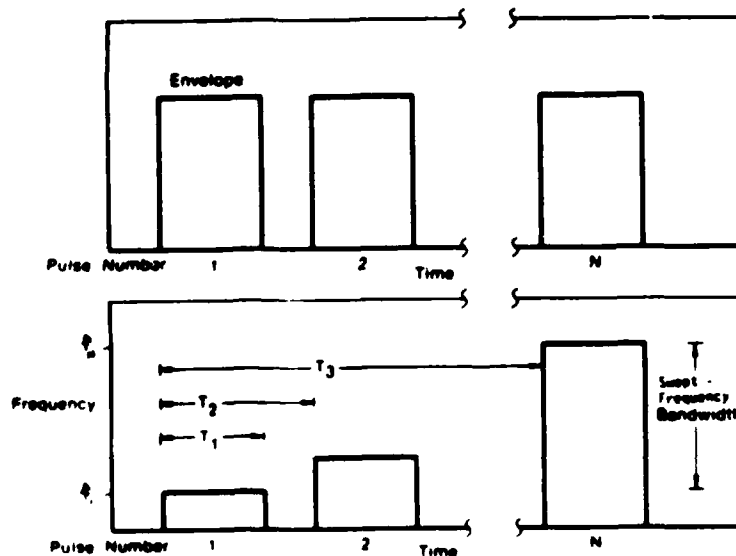
Figure 2.3. The Stepped-Frequency Pulse Burst

Each succeeding pulse in the burst is stepped in frequency. The separation between pulses is large enough for the transmitted pulse to travel to the target and the echoed pulse to return to the receiver before the next pulse is transmitted. This is illustrated in Figure 2.4, showing the relative delay of an echo from a point target compared to the time interval between transmitted pulses. The interpulse spacing is referred to as time T_2. The duration of the burst, referred to as time T_3, is the same length as a linear-FM pulse, yielding the same doppler resolution. This comparison is based on the formula for cross-range resolution, from (3),

$$\Delta x = \frac{\lambda}{4\sin(\theta/2)} \approx \frac{\lambda}{2\theta} = \frac{\lambda}{2\omega_r NT_3} \quad .$$

For a linear-FM pulse waveform, λ is the wavelength of the center frequency, whereas for a stepped-frequency pulse-burst, λ is the wavelength of the lowest frequency in the burst. The total angle rotated by the target is θ, and target angular velocity is ω_r.
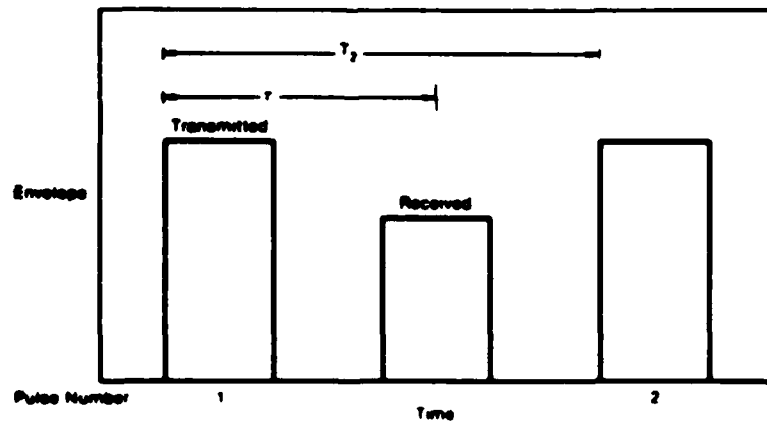
Figure 2.4 Rotation of Transmitted and Received Pulses
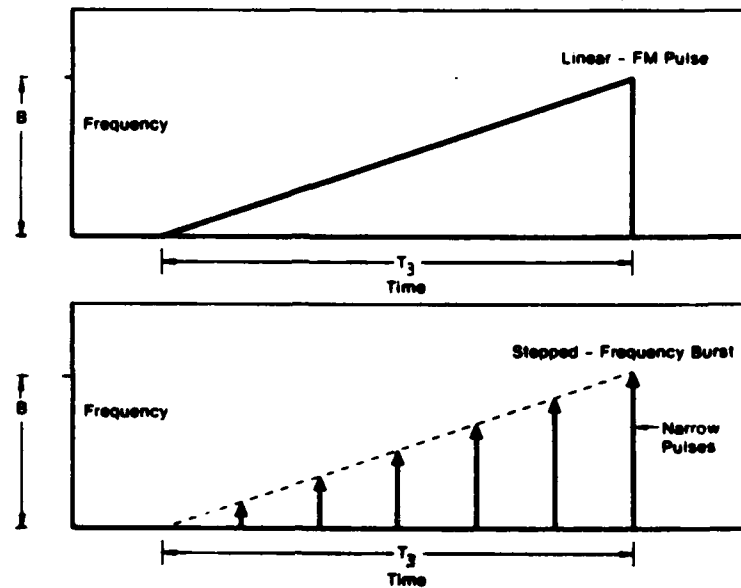
Figure 2.5. Comparison of Pulse Burst With Linear-FM Pulse

In Figure 2.5, the stepped-frequency burst of pulses is compared to the
linear-FM pulse, showing the same swept-frequency bandwidth transmitted
during the respective waveforms. This bandwidth is the same for each,
to yield equal delay resolution. The equation for delay resolution is
as follows, from (3),

$$\Delta y = \frac{c}{2B} \quad ,$$

where B, also used in Figure 2.5, is the swept-frequency bandwidth of
the linear-FM pulse and the stepped-frequency burst and c is the speed
of light. It is seen that the stepped-frequency burst is a discretized
version of the linear-FM pulse. Each pulse in the stepped-frequency
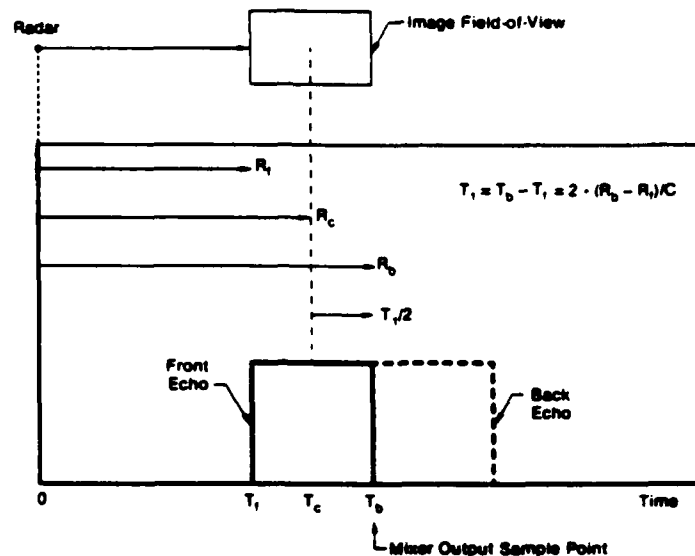
Stepped-Frequency Pulse Width Coverage

Figure 2.6

waveform has duration T_1, chosen to correspond to the two-way travel time of a signal across the field of view of the image along the delay dimension. This arrangement enables the following situation, as illustrated in Figure 2.6. The reflected pulse arriving at the receiver can be considered to be composed of component pulses reflected by resolution cells distributed in delay. By measuring the mixed received signal at the instant of time $T_1/2$ seconds after the round-trip delay to the center of the image area, illustrated as τ in Figure 2.6, the mixer output, a complex quantity, will be the sum of received signal components from each resolution cell in the target. A measurement of the complex signal is made in this fashion for each return pulse, after mixing with the transmitted pulse, resulting in a sequence of complex numbers for each burst of pulses.

Several bursts are transmitted to produce an image. The sequence of received measurements for each burst can be placed in rows of a two dimensional array in the same way as linear-FM processing. The rows represent the spectrum of a range profile of the target and, when the inverse Fourier transform is computed, result in the complex range profile. To generate an image, the forward Fourier transform magnitude of each column is computed, as it was for the linear-FM technique, to sort doppler frequency components into a cross-range profile. The result is a two dimensional image.

There are several advantages to using the stepped-frequency technique to make ISAR images. Since a narrow pulse of constant frequency is the basic unit of the waveform, with each of these separated by a relatively long time interval, the wide instantaneous bandwidth and high sampling rate requirements of transmit and receive equipment is removed compared to what is necessary for the linear-FM technique. The stepped-frequency ISAR technique is far simpler to implement for this reason.

2.3 ANGULAR DOPPLER PROCESSING

As described by Mensa (2), in the stepped-frequency waveform and linear-FM waveform, and associated imaging techniques, there can be seen a duality of time and angle of the target during signal transmission. The target rotates continuously and there is a one-to-one correspondence between time and angular position. Therefore, the Fourier transforms, which were before seen as operations on temporal signals, can also be viewed as transforms of spatial signals.

Making use of this concept means that the stepped-frequency ISAR approach can be used in a laboratory setting to make two dimensional

radar images without having to rotate the target continuously. The target's angular position is merely incremented without regard to time. Also, it is not necessary to use narrow pulses at all, but merely to reflect a continuous wave signal of specified frequency off the target and measure the mixer output from the received continuous wave signal. Continuous wave transmission and reception equipment is simpler than the equipment necessary for pulsed operation and means that a laboratory implementation is relatively easy to construct. Laboratories use this angular doppler technique to two-dimensionally map, with high resolution, the radar cross-section of targets.

3. ALGORITHM IMPLEMENTATION

A computer program was developed which implements stepped-frequency ISAR imaging. This was implemented as a simulation of radar imaging, so targets were specified and their scattering functions were determined analytically. The computer program uses the scattering function to calculate the mixed received signal from the target. The ISAR processing part of the simulation uses the received signals to generate an image. This simulation was implemented in the facilities of the Electronic Systems and Signals Research Laboratory at Washington University. The radar images obtained were displayed on a color graphics display. To accomplish this, it was necessary to study the mathematical model of ISAR processing. This model is presented in this chapter. Also described are computer algorithms which implement the radar imaging simulation. Finally, the results of the radar imaging simulation are presented by examples of images which were generated.

3.1 DISTRIBUTED TARGET MODEL

The objective is a high resolution image of the radar target. The target is distributed over many resolution cells. When the entire target is illuminated by the radar, the target is within the antenna beam width, and the back-reflected signal is considered to consist of the superposition of the returns from the multitude of resolution cells. Each resolution cell appears as a point scatterer. Thus, the target can be viewed equivalently as an array of point scatterers which produces the same radar return as the actual target. For the disk and spherical targets, the resolution cells are located on the surface as shown in

Figure 3.1 where one such resolution cell is located as an intersection in delay and doppler. In the front view of the target shown in Figure 3.1, the radar illuminates the target from a position perpendicular to the plane of the paper.
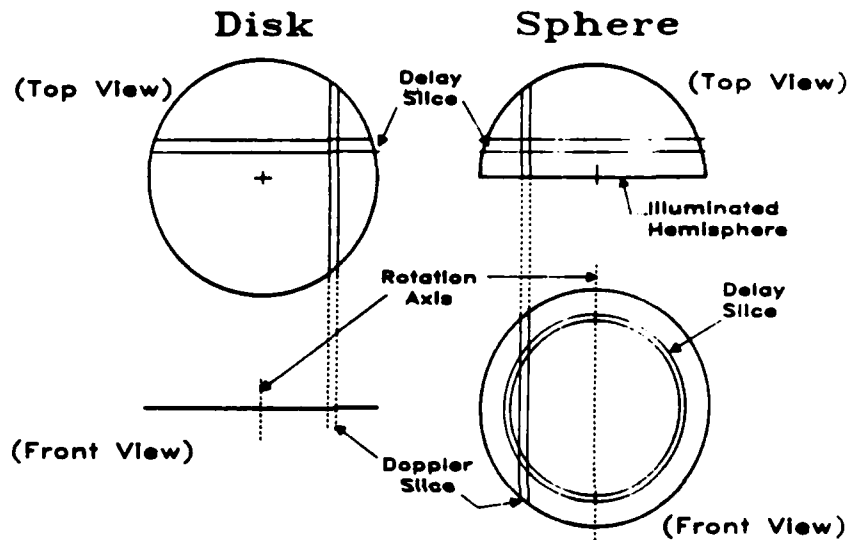
Figure 3.1 The Disk and Sphere Targets

In fact, for the spherical target, there are two area elements on the surface with the same delay-doppler coordinates. This is an ambiguity resulting from the geometry of the situation and the properties of high resolution radar. The radar resolves the three dimensional target surface in only two dimensions, delay and doppler. The total reflection of the resolution cell is the sum of the reflection of the two area elements.
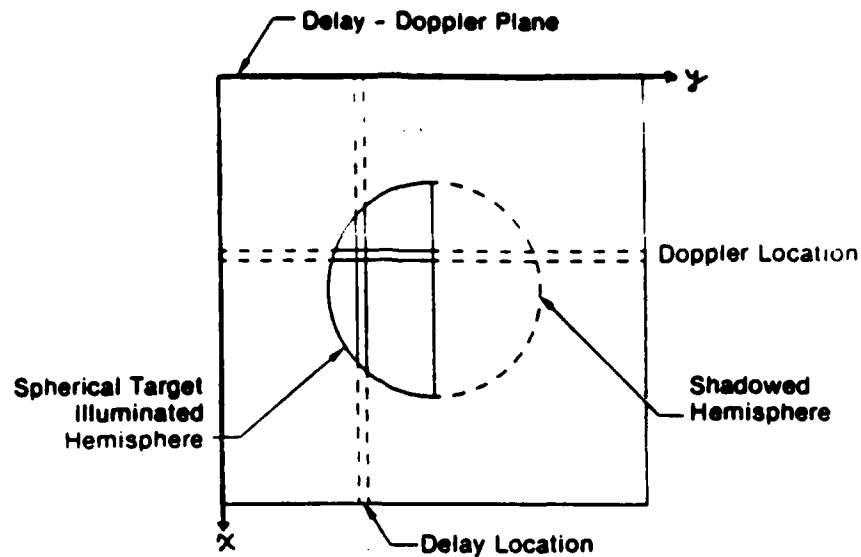
Figure 3.2. The Delay-Doppler Plane

The two area elements of the resolution cell are equivalently mapped onto the delay-doppler plane shown on Figure 3.2. Point scatterers on the delay-doppler plane can represent the resolution cells mapped onto it. The reflectivity of a point equals the vector sum of reflectivity within the resolution cell, as described in (3).

The two-dimensional planar array of points of reflectivity squared magnitude is called the scattering function of the target. The signal which would be received from an illumination of the point scatterers in the scattering function is equivalent to the back scattered signal from the actual target. However, the following assumptions are imposed on the reflectivity of the points during ISAR imaging, as described in (4). It is assumed the reflectivity does not change over the bandwidth of illuminating signals. Also, it is assumed the reflectivity does not change as target aspect changes with rotation during the sequence of pulses necessary for an image.

3.2 STEPPED-FREQUENCY ISAR PROCESSING MODEL

At the instant of mixer output measurement specified as T_b in Figure 2.6, the received signal is comprised of the superposition of components echoed from the point scatterers in the target. The superposition occurs over the delay-doppler plane as follows. The whole received signal,

$$\tilde{s}_i(t) = \sum_{u,v} \tilde{s}_r(t),$$

where u is the delay location, v is the doppler location, and t is the time.

The received signal component due to a resolution cell reflection is,

$$\tilde{s}_r(t) = \tilde{b} \, \tilde{s}_T(t-\tau),$$

where τ is the travel time delay, and $\hat{b}$ is reflectivity at the delay-doppler coordinate. This received signal is a reflection of the transmitted signal,

$$\tilde{s}_T(t) = \tilde{f}(t) \, e^{j \, 2\pi f_i t},$$

where i is the pulse number, f_i is the frequency of the pulse, and $\tilde{f}(t)$ is the complex envelope of the transmitted pulse. Assume $\tilde{f}(t) = 1.0$ within the pulse.

For the discussion in this section, the reflectivity is assumed to be a real number and a deterministic value equal to the square root of $\lambda(u,v)$, reflected power in the resolution cell at the delay-doppler coordinate (u,v). The quantity $\lambda(u,v)$ is also called the scattering function. In this section, the processing is shown to map correctly the delay-doppler reflected power, a non-randomly fluctuating quantity. This will verify the proper operation of the processing.

If ISAR processing works correctly, it reconstructs from the received signals the scattering function which produced them. Because of the linear superposition property of the Fourier transform, the imaging of the entire scattering function is the sum of the imaging of single point scatterers. Therefore, consider a single point scatterer and the received signal from a pulse reflected from it,

$$\tilde{s}_i(t) = b \; e^{j \; 2\pi f_i(t-\tau)}, \; b \text{ is real.}$$

This signal is a complex quantity consisting of real and imaginary, alternatively in-phase and quadrature, components. To get an ISAR image of the single point, the first step is the mixing of the received signal with the transmitted signal. This is accomplished by the system shown in Figure 3.3.
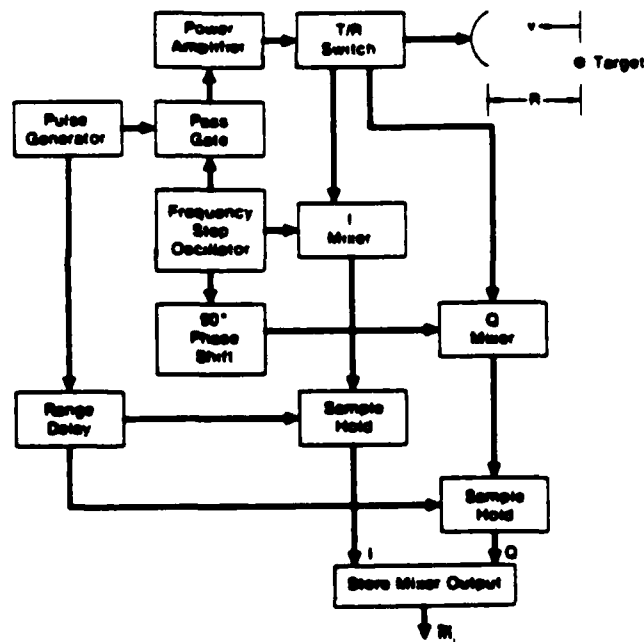
Figure 3.3. The Stepped-Frequency ISAR System

The mixer output is derived as follows. At the instant of measurement the mixer output signal,

$$\tilde{m}_i(t) = 2 \cdot LP[Re(\tilde{s}'_i(t)) \cdot Re(\tilde{s}_T(t))] + j \ 2 \cdot LP[Im(\tilde{s}'_i(t)) \cdot Im(\tilde{q}(t))],$$

where LP means a low-pass filter, $\tilde{s}'_i$ is the received signal, $\tilde{S}_T$ is the transmitted signal, and $\tilde{q}' = \tilde{S}_T$ shifted 90° $= j \ \tilde{S}_T$.

In the first term,

$$Re[\tilde{s}_i(t)] \cdot Re[\tilde{s}'_T(t)] = b \cos 2\pi f_i(t-\tau) \cdot \cos 2\pi f_i t$$

where Re[ ] means the real part is taken. Since

$$\cos(at) \cdot \cos(bt) = \frac{1}{2}[\cos(a+b)t + \cos(a-b)t],$$

it follows that

$$Re[\tilde{s}'_i(t)] \cdot Re[\tilde{s}'_T(t)] = \frac{b}{2}[\cos 2\pi f_i(2t-\tau) + \cos 2\pi f_i \tau].$$

Similarly, since $\sin(at) \cdot \cos(bt) = \frac{1}{2}[\sin(a+b)t + \sin(a-b)t]$, in the imaginary term of the mixer output signal,

$$Im[\tilde{s}_i(t)] \cdot Im[\tilde{q}_i(t)] = b \sin 2\pi f_i(t-\tau) \cdot (-\cos 2\pi f_i t),$$

$$= \frac{b}{2}[-\sin 2\pi f_i(2t-\tau) - \sin 2\pi f_i(-\tau)],$$

$$= \frac{b}{2}[-\sin 2\pi f_i(2t-\tau) + \sin 2\pi f_i \tau],$$

where Im[ ] means the imaginary part is taken. After low-pass filtering, the real component of the mixer output signal is given by

$$2 \cdot LP[Re(\tilde{s}'_i(t)) \cdot Re(\tilde{q}'_i(t))] = b \cos 2\pi f_i \tau.$$

Also, after low-pass filtering, the imaginary component of the mixer output signal is given by

$$j \ 2 \cdot LP[Im(\tilde{s}'_i(t)) \cdot Im(\tilde{q}_i(t))] = j \ b \sin 2\pi f_i \tau.$$

Therefore, the total mixer output signal is given by

$$\tilde{m}_i(t) = b \cos 2\pi f_i \tau + j\, b \sin 2\pi f_i \tau,$$

or,

$$\tilde{m}_i(\tau) = b\, e^{j\, 2\pi f_i \tau}.$$

For a single point target of arbitrary location in the delay-doppler field of view, the round-trip delay τ is given by

$$\tau = \tau(t) = \frac{2}{c}(r - v_r t),$$

where v_r is relative velocity of the point target, and r is initial range to target.

There are a fixed number of pulses in a burst, yielding a sequence of mixer output values. Time within the burst is incremented as follows:

$$t = i\, T_2 + T_1/2 + k\, T_3,$$

where k is Burst index, T_1 is pulse width, and i is the pulse index. Using this equation for time in the above equation for round-trip delay, τ may be expressed as

$$\tau = \frac{2}{c}(r - v_r(i\, T_2 + T_1/2 + k\, T_3)).$$

The expression for the mixer output signal then becomes,

$$\tilde{m}_i = b\, \exp[j\, 2\pi f_i\, \frac{2}{c}(r - v_r(i\, T_2 + T_1/2 + k\, T_3))],$$

where exp [ ] means an exponential function.

The sequence of mixer outputs from a burst is inverse Fourier transformed to get a range profile RP(n) of the target,

$$RP(n) = IDFT[\tilde{m}_i] = \frac{1}{N} \sum_{i=0}^{N-1} \tilde{m}_i \, e^{j \frac{2\pi}{N} i \, n},$$

where N is the number of pulses, n is the range profile index, IDFT means an inverse discrete Fourier transform is computed. Substituting the expression for the mixer output signal in this range profile equation, it is seen that

$$RP(n) = \frac{b}{N} \sum_{i=0}^{N-1} \exp[j \, 2\pi f_i \, \frac{2}{c} \, (r - v(i \, T_2 + T_1/2 + k \, T_3))] \exp[j \frac{2\pi}{N} i \, n],$$

or after rearranging terms,

$$RP(n) = \frac{b}{N} \sum_{i=0}^{N-1} \exp[j \frac{2\pi}{N} (i \, n + N f_i \frac{2}{c}(r - v_r(i \, T_2 + T_1/2 + k \, T_3)))].$$

The frequency of any pulse is expressed as, $f_i = f_0 + i \, \Delta f$, where f_0 equals initial frequency used in the burst and Δf is the frequency step of the succeeding pulses. It follows that

$$RP(n) = \frac{b}{N} \sum_{i=0}^{N-1} \exp[j \frac{2\pi}{N} (i \, n + \frac{2N}{c}(f_0 + i \Delta f) (r - V_r(i \, T_2 + T_1/2 + k T_3)))].$$

By using $N \Delta f = B$, and $\frac{2B}{c} = \frac{1}{\Delta r}$, the above expression for the range profile is simplified. Also, the following restriction on point target motion is imposed,

$$|v_r(i T_2 + T_1/2 + k T_3)| < \Delta r,$$

where Δr is range resolution. This restriction implies that the point does not move out of its resolution cell during rotation. This results in the following expression for the range profile,

$$RP(n) = \frac{b}{N} \sum_{i=0}^{N-1} \exp[j \frac{2\pi}{N} (i\ n + \frac{ir}{\Delta r} + Nf_o \frac{2r}{c})]. \tag{3.1}$$

Since $\frac{r}{\Delta r} = -n_o$, and $\frac{2r}{c} = \tau_k$, it follows that

$$RP(n) = \frac{b}{N} e^{j\ 2\pi f_o \tau_k} \sum_{i=0}^{N-1} e^{j \frac{2\pi}{N} i(n-n_o)} , \tag{3.2}$$

where τ_k is a delay time associated with a particular burst. The resulting range profile is then from (3),

$$RP(n) = b\ e^{j\ 2\pi f_o \tau_k} \frac{\sin \pi(n-n_o)}{\sin \frac{\pi}{N}(n-n_o)}$$

The range profile sequence has a function narrow "impulse-like" term which has peak response within the down-range resolution cell where the point target is located, low-level sidelobes next to the peak and essentially zero response in other positions. Each burst has a range profile described by the above equation, containing a phase term which is a function of burst number and target velocity. In the following, the above equation is simplified by replacing the narrow "impulse-like" function term with an ideal impulse which is unity within the down-range resolution cell of the point target and zero in other positions, thus ignoring the low-level sidelobes of the above response.

In this manner, the above equation is expressed as,

$$RP(n) = b\ e^{j\ 2\pi f_o\ \tau_k}\ \delta(n-n_o) \tag{3.3}$$

In the next step of ISAR processing, the point target is located in cross-range position by taking the discrete Fourier transform (DFT) of the sequence of range profile values of constant range,

$$DFT \; [RP(n_o)] = \sum_{k=0}^{N-1} b \; exp[j \; 2\pi f_o \tau_k] \; exp[-j \; \frac{2\pi}{N} \; km].$$

This is described as a cross-range profile,

$$CRP(m) = b \sum_{k=0}^{N-1} exp[-j \; \frac{2\pi}{N} \; (mk - Nf_o \tau_k)],$$

where m is the doppler index of the sequence and $\tau_k = \frac{2}{c} (r - V_r \; k \; T_3)$.

Using this expression for burst delay time in the cross-range profile results in

$$CRP(m) = b \sum_{k=0}^{N-1} exp[-j \; \frac{2\pi}{N} \; (km - Nf_o \; \frac{2r}{c} + kT_3 \; \frac{2}{c} \; V_r Nf_o)].$$

By separating out the constant phase term, $\tau = \frac{2r}{c}$, and inserting $f_o = \frac{c}{\lambda}$, the cross-range profile becomes,

$$CRP(m) = b \sum_{k=0}^{N-1} exp[-j \; \frac{2\pi}{N} \; k(m + NT_3 \; \frac{2}{\lambda} \; V_r)] \; exp[j \; 2\pi f_o \tau].$$

Since $V_r = m_o \; \Delta x \; \omega_r$,

$$CRP(m) = b \; exp[j \; 2\pi f_o \; \tau] \sum_{k=0}^{N-1} exp[-j \; \frac{2\pi}{N} \; k(m - \frac{NT_3 2}{\lambda} \; m_o \; \Delta x \; \omega_r)].$$

Using $\Delta x = \frac{\lambda}{2\omega_r \; NT_3}$,

$$CRP(m) = b \; e^{j \; 2\pi f_o \tau} \sum_{k=0}^{N-1} e^{-j \; \frac{2\pi}{N} \; k(m - m_o)} = be^{j \; 2\pi f \tau} \; [\frac{sin \; \pi \; (n-n_o)}{sin \; \frac{\pi}{N} \; (n-n_o)}].$$

By retaining only the peak impulse response and ignoring low-level sidelobes,

$$CRP(n) = b \, e^{j \, 2\pi f_o} \, \delta(m-m_o).$$

The magnitude of the cross-range profiles forms the image. When simplifying the expression by ignoring side-lobes and using only the ideal impulse peak response, the profile magnitudes form an image,

$$|CRP(m)| = Image \, (n,m) = b \, \delta(n-n_o, \, m-m_o).$$

This is the final result of ISAR processing. It is seen that the point target shows up in the image at delay-doppler coordinate $(n_o, \, m_o)$ as a point with magnitude equal the square root of the scattering function, as it is supposed to.

For some parameter choices, the total angle of target rotation during the image frame time is more than a few degrees. In this case, the point target described above will migrate out of its resolution cell during the image frame time, invalidating the assumption used in getting equation 3.1 above. The effect will be a distorted image. This problem is described in (3) and is known as "range walk". A resulting image will appear as if each range profile is staggered in position relative to its neighbor. This distortion is corrected by multiplying the mixer output samples by a correction factor derived here.

Compensating for the range walk problem results in the following modification of equation 3.1,

$$RP(n) = \frac{b}{N} \, \sum_{i=o}^{N-1} \, \exp[j \, \frac{2\pi}{N} \, (i \, n + \frac{i}{\Delta r} \, (r - VkT_3) + \frac{2Nf_o}{c} \, (r - VkT_3))].$$

This range profile equation can be reduced to,

$$RP(n) = \frac{b}{N} \exp[j \frac{2\pi}{N} f_o \tau_k] \sum_{i=0}^{N-1} \exp[j \frac{2\pi}{N} i((n-n_o) - k \frac{VT_3}{\Delta r})]. \qquad (3.4)$$

By representing the response as an ideal impulse and ignoring low-level sidelobes, this range profile is expressed by the following function additionally dependent on burst number,

$$RP(n, k) = \frac{b}{N} \delta (n-n_o - k \frac{VT_3}{\Delta r}).$$

This expression for the range profile looks like that in equation 3.3, on page 22, except that for each succeeding burst, the profile position is offset in range position by a term due to target motion between bursts. This is corrected by multiplying the mixer output sequence for a burst by a correcting factor prior to computing the transform. This modifies equation 3.4 so that it looks like equation 3.2, resulting in a corrected range profile,

$$RP(n) = \frac{b}{N} \exp[j \frac{2\pi}{N} f_o \tau_k] \sum_{i=0}^{N-1} \exp[j \frac{2\pi}{N} i(n-n_o - k \frac{VT_3}{\Delta r})]S_{ik},$$

where S_{ik} is the range walk correction which equals

$$\exp[j \frac{2\pi}{N} ik \frac{VT_3}{\Delta r}]. \quad \text{Then,}$$

$$RP(n) = \frac{b}{N} \exp[j \frac{2\pi}{N} f_o \tau_k] \sum_{i=0}^{N-1} \exp[j \frac{2\pi}{N} i((n-n) - k \frac{VT_3}{\Delta r})]\exp[j \frac{2\pi}{N} ik \frac{VT_3}{\Delta r}]$$

$$= \frac{b}{N} \exp[j \frac{2\pi}{N} f_o \tau_k] \sum_{i=0}^{N-1} \exp[j \frac{2\pi}{N} i(n-n_o)].$$

From this, it is seen that the range walk correction factor does restore the range profile to the proper form.

3.3 COMPUTER SIMULATION

A FORTRAN program was written to achieve the goal of producing ISAR images in the laboratory by simulation. The dimensions of simulated targets were specified, and their scattering functions were supplied for use. The simulation contained two parts. The first part inputs the scattering function and calculates the mixer output signals from that target for all pulses and bursts transmitted. The second part processes the signals using Fourier transform techniques, as described here, to produce an image data file. An image display routine is used to display the simulated ISAR image on a color monitor.

An algorithm is presented in Figure 3.4 to describe the programming of the part of the simulation which calculates mixer output signals.

```
Read in Scattering Function
Increment Burst Number m
|  K=1
|  Increment Resolution Cell  (τ, f) = (i, j)
|  |  Increment Pulse Number n
|  |  |  Calculate Received Signal S(n)
|  |  |  S_k(n) = S_{k-1}(n) + S(n)
|  |  End Loop
|  |  K = K + 1
|  End Loop
|  Store S(n) in S(n, m)
End Loop
Normalize S(n, m) to max [S(n, m)] = 1.0
End
```

Algorithm of Mixer Output Simulation

Figure 3.4

A two-dimensional array is used to store the resulting radar signals; each burst forms a row of the array.

Two analytic targets were chosen, a rough disk and a rough sphere. The field-of-view of the image was chosen to be 76.8 meters in both range and cross-range dimensions. The resolution in both dimensions was chosen to be 60 centimeters. The scattering function is a 128 by 128 array of reflected power values. The diameters of both the disk and sphere were chosen to be 38.4 meters with both centered in the field-of-view. It was desired to write a computer program that would generate an image of size 256 pixels on each side with the same resolution of 60 cm in each coordinate. This is accommodated in the Fourier transform techniques by padding with zeroes. This results in an image that is magnified by a factor of two and is easier to see on the color monitor.

In this simulation, 128 pulses per burst and 128 bursts are used in the transmitted waveform. This covers the field-of-view of interest, given the resolution. The resulting two-dimensional array holding the mixer output signal is of size 128 by 128. The range profiles are calculated with an inverse discrete Fourier transform (DFT). This procedure uses a subroutine for DFT calculation which was supplied by the University. Also in computing a range profile, the 128 point signal is placed in the center of a 256 point array, padded on both ends with 64 zeroes, for the inverse DFT operation. The resulting 256 point range profile, divided by the number of points, replaces the row of signal data in the two-dimensional array.

In the final step of calculations, the cross-range profiles of the image are made using a forward DFT on the columns of the two-dimensional array resulting from the last operation. However, rearrangement of the data in the 256 point array is necessary. Instead of placing the 128 data points in the center of the 256 point array, the first 64 data points are put in the first 64 array locations and the last 64 data points are placed in the last 64 array locations, leaving the center array locations zeroed. This is due to the way the DFT routine operates. After the DFT is computed, the zero frequency location is in the first array location, so the data are rearranged with the last half of the 256 points switched with the first half. This is illustrated in Figure 3.5. The squared magnitudes of the resulting complex numbers are stored in each column of the two-dimensional array. The resulting two-dimensional image data array is used with a color scale to display the image.
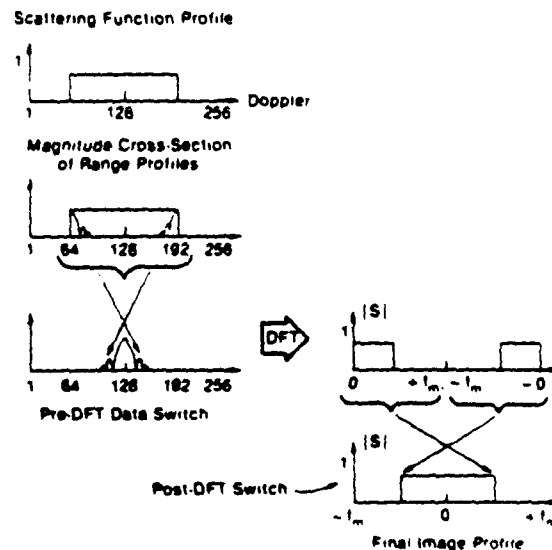
Figure 3.5. Fourier Transform Techniques

The computer listing is included in the Appendix in Figure 7.1. In the main routine, PROC3, the target's scattering function is input and the mixer output signal is calculated. This signal is normalized to peak magnitude. Subroutine IMAGE2D is then called to reconstruct the image.

As a part of this simulation development, a modification of the Fourier transform techniques described above was investigated. A modified IMAGE2D subroutine was constructed in which the Fourier transforms were "windowed" with a normal function,

$$w(n) = e^{-0.09 (n-N/2)^2} \text{ , } n = \text{index, } N = 128.$$

Windowing is described as multiplying the complex data sequence by the window function before calculating the transform. Due to the symmetry properties of the Fourier transform, each of the delay and doppler transforms are windowed with the same function. This modified routine is called IMAGE2DW and is listed in the appendix.

3.4 COMPUTER FACILITIES

The computer program was written in FORTRAN or a Massachusetts Computer Company (MASSCOMP) image processing computer, model MC500, with a color graphics display terminal. The color of the pixels in the raster display are controlled by a color scale with 64 intensity levels. A heated object color scale was chosen. Once a two-dimensional array of data is available, an image display routine is executed which reads the data and generates the image or the screen. A picture of this facility is presented in Figure 3.6.
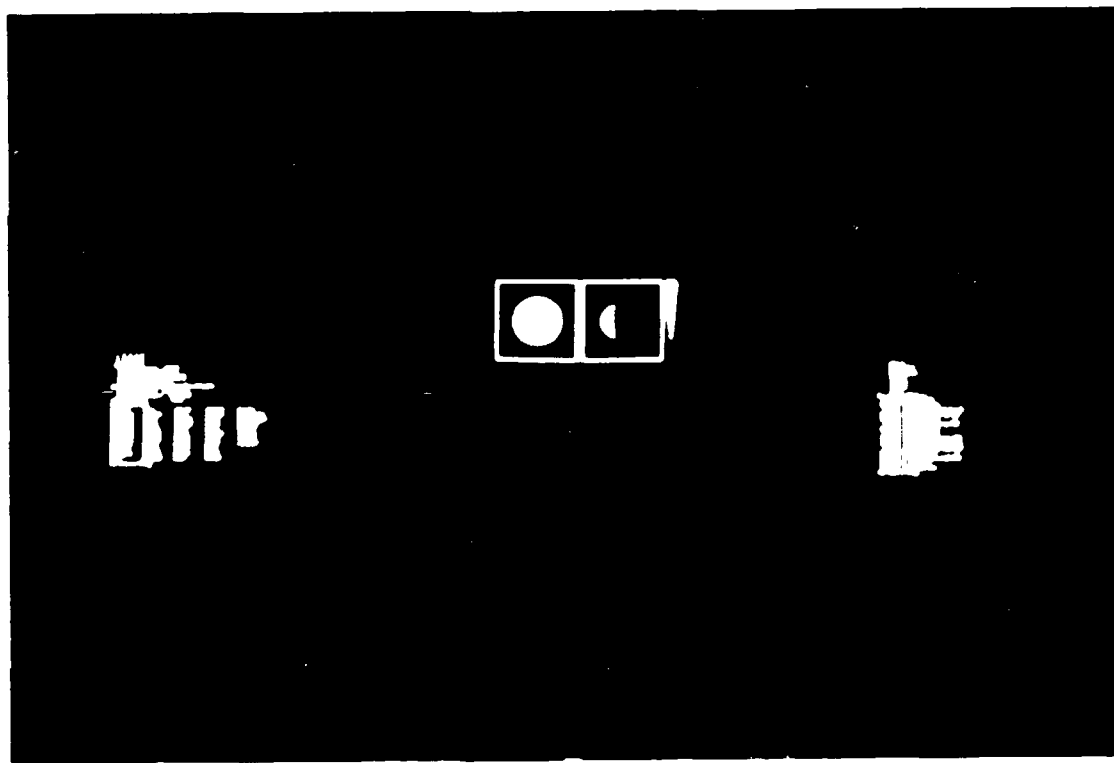
Photograph of Computer Facilities

Figure 3.6

3.5 SIMULATION RESULTS

Several scattering functions with the same resolution and size were used in tests of the ISAR imaging simulation. These scattering functions can be displayed to see what the actual target looks like. Their data arrays are sized 128 by 128, but it is desired to see them as a 256 by 256 pixel image. Therefore one data point drives 4 pixels in order to double the size of the image. As first test cases, point target pairs were used. One pair has a point in the center of the image, at location (64,64) of the 128 by 128 scattering function, and a point at (64,96). Another point target pair uses a center point and a point at (64,66). The ISAR imaging simulation was used to reconstruct ISAR images of the scattering functions. These radar images are displayed in Figure 3.7 with the closely spaced pair on the left (a). The resulting images are 256 by 256 pixels in size due to the processing implementation described above. The fact that the radar images look like the scattering functions confirms the proper operation of the ISAR processing for these test targets.

(a)   (b)
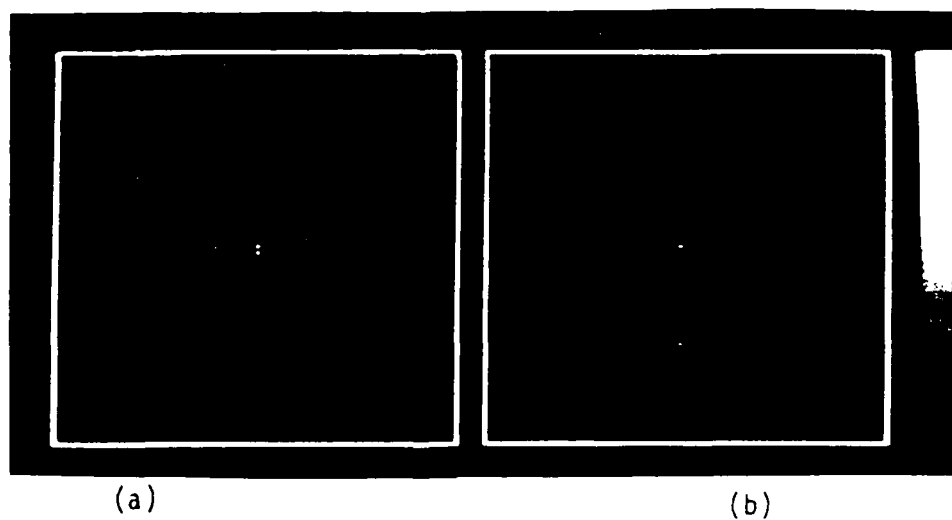
ISAR Images of Point Target Pairs

Figure 3.7

During image display, the image data is scaled to the color scale so that the peak value is shown as white and zero values appear as black. In the images in Figure 3.7, the peaks of the responses from the point targets are seen very well. However, there are also sidelobes to the peaks which are subdued in these pictures by the color scale and the effects of film processing.

The scattering functions of the rough disk and rough sphere are displayed in Figure 3.8. These scattering functions come from reference (1). The disk is shown on the left (a) in the figure. Note that the sphere (b) shows the effects of shadowing which makes the illumination look somewhat like a partial moon. Also, the reflected power is greatest from the point on the target closest to the radar and decreases for points closer to the shadowed edge. In this figure and in other similar images shown here, the radar is illuminating from the left side.

(a)   (b)
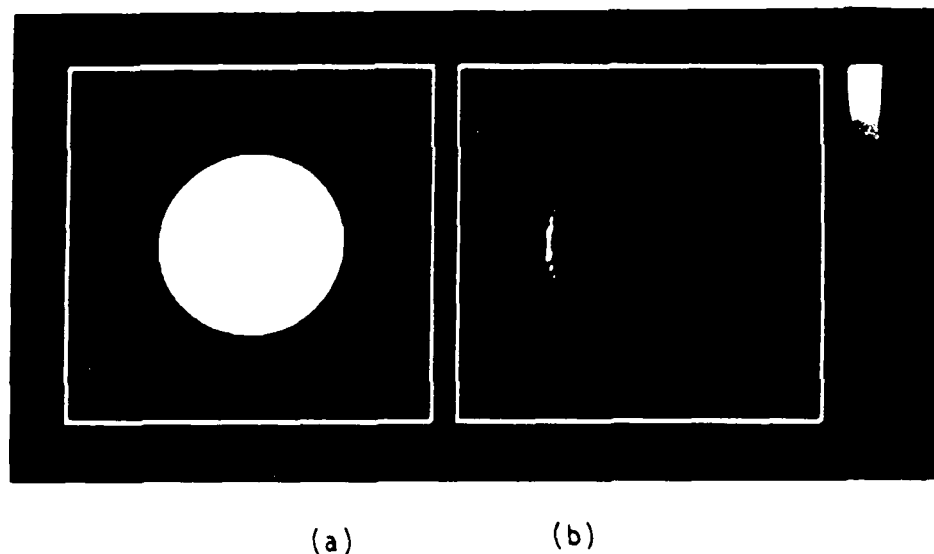
Scattering Functions of Disk and Sphere

Figure 3.8

Reconstructed images of the disk and sphere are presented in Figure 3.9. Horizontal corresponds to the delay dimension and vertical to the doppler dimension. Note that the sphere's image (b) looks like that in Figure 3.2. The disk's image is on the left (a) in Figure 3.9. There is substantial low-level sidelobe energy in the image which can be smoothed out by windowing, but results in a loss of resolution.

(a)   (b)
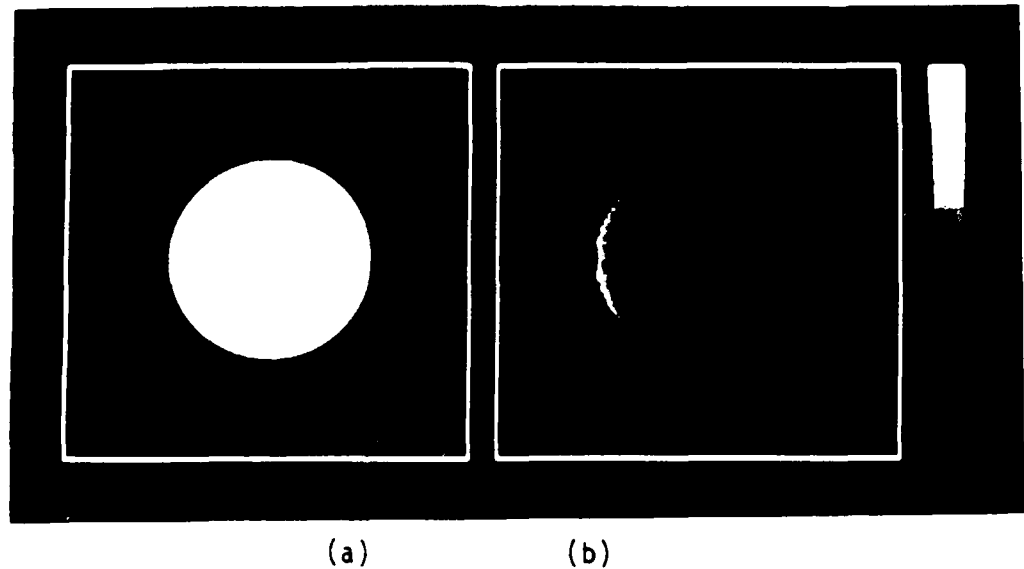
ISAR Images of Disk and Sphere

Figure 3.9

An image of a center located point target, reconstructed using windowed transforms is shown in Figure 3.10. The window is described at the end of Section 3.3. As can be seen, windowing blurs a point target. The profile of the image is also plotted in the figure. The plot also shows the form of the window. A similarly windowed image of the spherical target is presented in Figure 3.11 along with the profile plot. Those images suggest that the blurring introduced by windowing reduces image quality, but side-lobe energy is reduced.
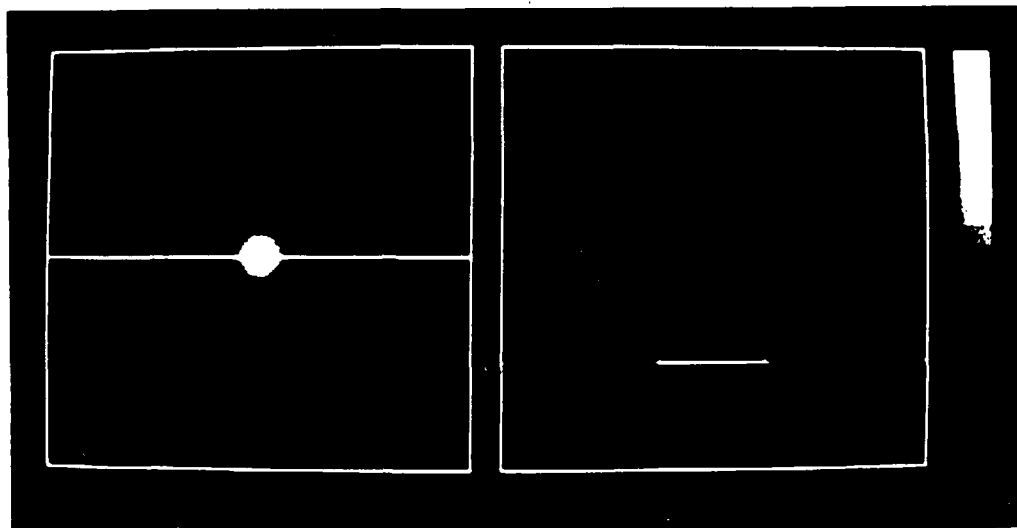
Windowed ISAR Image of Center Point Target

and Profile Plot

Figure 3.10
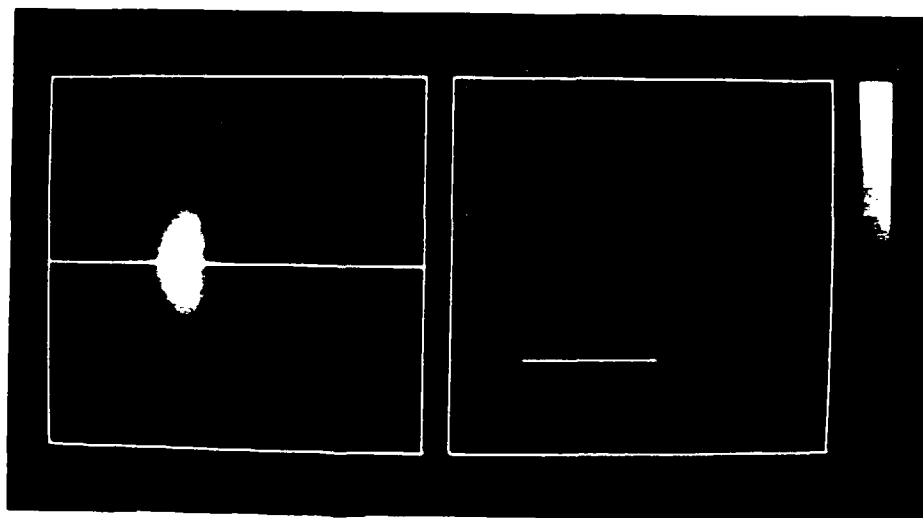
Windowed ISAR Image of Spherical Target

and Profile Plot

Figure 3.11

4. STATISTICAL TARGET MODEL

In the preceding chapter, the reflectivity of the target surface, for each resolution cell, was taken to be a fixed real value equal to the square root of the scattering function value. This was for the purpose of verifying the ISAR processing. The next desired step was to image a diffuse target surface. The reflectivity of a diffuse target is a complex random process.

The resolution cells are distributed in the delay-doppler plane. Each is described as a slowly fluctuating point target in the presence of additive noise. The resolution cell is made up of several reflecting surfaces which combine to produce a random reflected signal. Slowly fluctuating means the reflectivity is partially correlated relative to the transmitted signal pulse burst period.

4.1 MODEL OF A SLOWLY FLUCTUATING POINT TARGET

The source for this model is Van Trees (5). The radar's transmitted signal is represented as follows:

$$\tilde{s}_T(t) = A \; \tilde{f}(t) \; \exp[j2\pi f_i t]$$

where $\tilde{f}(t)$ is the normalized complex envelope of transmitted signal, A is the amplitude, and f_i is the carrier frequency. The power of such a signal is A^2, from (6,7).

Consider a point target in space, representing a resolution cell in the delay-doppler plane with zero velocity. The reflected signal from such a target includes the effect of the random reflectivity process.

This noise source is multiplicative and the received signal can represented as follows:

$$\tilde{s}_r(t) = \tilde{b} \; \tilde{f}(t-\tau) \; \exp[j \; 2\pi f_i(t-\tau)],$$

where τ is round trip delay. The term $\tilde{b}$ is a complex Gaussian random variable with zero mean. The variance of the real and imaginary components is equal to half the power of the reflected signal. A point target with non-zero velocity will have the same form of reflected signal, but the carrier frequency will be shifted by the Doppler effect.

A target which is extended in the delay-doppler plane, and slowly fluctuating, is considered to be composed of an array of point targets representing the resolution cells, each contributing a reflected signal of the above form. So, the total received signal from such a target is the sum of the received signals from each point target. Representing this sum and the additional feature that the signal has a doppler frequency shift, the received signal can be expressed as,

$$\tilde{s}_r(t) = \sum_{u,v} \tilde{b} \; \tilde{f}(t-\tau_u) \; \exp[j(\omega_i + \omega_r)t],$$

where $\omega_r = \omega_i \frac{2v_r}{c}$ is the doppler frequency, $\omega_i = 2\pi f_i$, the transmitted frequency, and (u,v) is an element of the delay-doppler plane.

The random reflectivity term has the property that it is wide-sense stationary and spatially uncorrelated. This property along with the slowly fluctuating property implies an approach in simulating the mixer output from a target.

For a resolution cell, the reflectivity from pulse to pulse is correlated by using a recursive filter. White Gaussian noise is filtered so it has a desired autocorrelation function. Two filters are

operated to generate separate outputs for each of the real and imaginary components of the reflectivity.

The following recursive filter was chosen from (8),

$$Y_n = aY_{n-1} + (1-a^2)^{1/2} X_n.$$

The input parameter X_n is a white gaussian variable which has a weighted contribution to the output value Y_n. The previous Y_{n-1} value has a weighted contribution to the output. The autocorrelation function of the filter output,

$$R_y(k) = R_x(o) \, a^{|k|} = \sigma_x^2 \, a^{|k|} \ .$$

The shape of the autocorrelation function is shown in Figure 4.1. The slope of the function near the peak is used to relate the parameter a to correlation interval parameter CI.
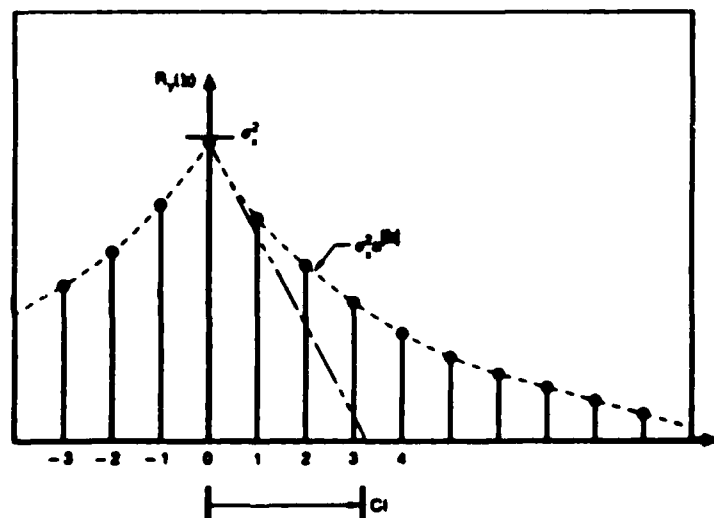
Figure 4.1 Reflectivity Autocorrelation Function

ISAR processing calculates the Fourier transform of the delay-doppler signal having random reflectivity. The result can be viewed as a convolution of the desired power density of the target with a poor estimate of the power spectrum of the random variable, as described in (6, Chapter 11, Section 3). This signal is itself a random process. The power spectrum of the correlated reflectivity components is given in (7,8,9),

$$S_y(k) = |H(k)|^2 \, S_x(k),$$

where $S_x(k)$ is the power spectrum of the white Gaussian noise, $S_y(k)$ is the power spectrum of the filtered noise and $H(k)$ is the filter's transfer function. However, the Fourier transform of a limited sample of a random process is itself a randomly varying quantity. So, the convolution results in random signal and resulting ISAR images are expected to look noisy.

The effects of additive noise are also to be included in the simulation of the received signal. Adding this term to the equation for the received signal yields the following:

$$\tilde{s}_r(t) = \sum_{u,v} \tilde{f}(t-\tau) \, \tilde{b} \, e^{j \, 2\pi f_i(t-\tau)} + \tilde{n}(t)$$

The last term is a complex gaussian random process with zero mean. It is included to model wideband channel and receiver noise. The first part of the signal is normalized to power equal 1.0, and the variance of the additive noise term is varied to produce a desired signal-to-noise power ratio (SNR),

$$SNR = \frac{P_s}{P_n} \, ,$$

where P_s and P_n are signal and noise power over the receiver bandwidth.

.

Further, SNR $= \dfrac{P_s}{P_n} = \dfrac{A^2}{B^2}$, where A is the signal amplitude, and since

$A^2 = 1$, then $B = 1/\sqrt{SNR}$. Thus the standard deviation of the real and

imaginary terms of complex white Gaussian noise are $B/\sqrt{2}$.

Because of the linearity of the Fourier transform, the result of

ISAR processing the above mixer output, with the additive noise, will

add to the image a signal which is the Fourier transform of the sampled

white gaussian noise. Since the noise is white, it is expected the

image will have noise added to it all over the field of view.

4.2 IMPLEMENTATION IN THE SIMULATION

The computer simulation, written in FORTRAN, was modified to calculate a received mixer output signal from a diffuse target. The scattering function of the target is input into the simulation, which is a delay-doppler mapping of the reflected signal power for each resolution cell. The target is slowly fluctuating, so the random reflectivity of each call of the scattering function is statistically correlated in time. This implies an outer loop which increments resolution cell. The algorithm of this computer program is presented in Figure 4.2.

```
Read in Scattering Function
Find Sum of Total Power within Scattering Function
Initialize 2D Array for Mixer Outputs to Zero (FRAME)

Increment Resolution Cell (i, j)
|    Initialize Random Reflectivity Recursive Filter
|    Increment Burst Number m
|    |    Increment Pulse Number n
|    |    |    Pick Correlated Random Reflectivity
|    |    |    Calculate Mixer Output S(n)
|    |    |    Sum Mixer Output to 2D Frame (n,m)
|    |    End Loop
|    End Loop
End Loop

Calculate Desired Noise Standard Deviation from SNR
Increment Burst Number m
|    Increment Pulse Number n
|    |    Pick White Gaussian Noise
|    |    Normalize Mixer Output
|    |    Add Noise to Mixer Output
|    End Loop
End Loop
End
```

Algorithm of Mixer Output Simulation
Using a Correlated Statistical Target
and Additive White Noise
Figure 4.2

For each resolution cell in the scattering function, one at a time, the mixer output for all pulses in all bursts is calculated using random number generators to get a complex Gaussian random number for reflectivity. The mixer outputs are stored in a two-dimensional array. The whole received signal is the point-to-point sum of two-dimensional arrays from each cell.

After all cells have been incremented, and the two dimensional array contains the mixer output resulting from the whole target, the mixer outputs are normalized to power equal 1.0. Then Gaussian random number generators are used for additive noise with power adjusted to get a desired signal-to-noise ratio.

Returning to the part of the algorithm where the mixer output for a pulse is calculated, the mathematics which is used to carry this out is developed in the following way. As described before, the received signal is composed of components from all resolution cells in the target and includes added noise. Assuming the received pulse's envelope $\tilde{f}(t-\tau)$ is unity, the received signal can be expressed as,

$$\tilde{s}_r(t) = \sum_{u,v} \tilde{b}\, e^{j(\omega_i + \omega_r)t} + \tilde{n}(t).$$

This signal $\tilde{s}_r(t)$ is mixed with $e^{j\,\omega_i\,t}$, the carrier signal, to give the mixer output signal which can be written as,

$$\tilde{s}_m = \sum_{u,v} \tilde{b}\, e^{-j\,\omega_r t} + \tilde{n}_m.$$

Letting $\theta_i = \omega_r t$, with i indicating pulse number, and

$\tilde{b} = \tilde{b}(u,v) = |b|e^{j\phi}b$ then,

$$\tilde{s}_m = \sum_{u,v} |\tilde{b}|e^{j(\phi_b - \theta_i)} + \tilde{n}_m .$$

Since $\cos(\phi_b - \theta_i) = \cos\phi_b \cos\theta_i + \sin\phi_b \sin\theta_i$,

and $\sin(\phi_b - \theta_i) = \sin\phi_b \cos\theta_i - \cos\phi_b \sin\theta_i$,

$$\tilde{s}_m = \sum_{u,v} \{(|\tilde{b}| \cos\phi_b \cos\theta_i + |\tilde{b}|\sin\phi_b \sin\theta_i)$$
$$+ j(|\tilde{b}|\sin\phi_b \cos\theta_i - |\tilde{b}|\cos\phi_b \sin\theta_i)\}.$$

Let $A = |\tilde{b}|\cos\phi_b$, and $B = |\tilde{b}|\sin\phi_b$, where A and B are Gaussian random variables with zero mean and variance $\sigma_A^2 = \sigma_B^2 = \frac{1}{2}$. $\lambda(u,v)$ then,

$$\tilde{s}_m = \sum_{u,v} \{(A \cos\theta_i + B \sin\theta_i) + j(B \cos\theta_i - A \sin\theta_i)\}$$

The computer program listing which incorporates this implementation of random reflectivity is presented in Appendix 7.1. The listing includes subroutines for random number generation which were supplied by the University. The function NRMRAN generates a normally distributed, uncorrelated random number of specified mean and variance equal 1.0. Zero mean was chosen, and the standard deviation is choosen to result in the desired power. The reflectivity is correlated from pulse to pulse by the subroutine SLATTER. However, the reflectivity of each resolution cell is made independent.
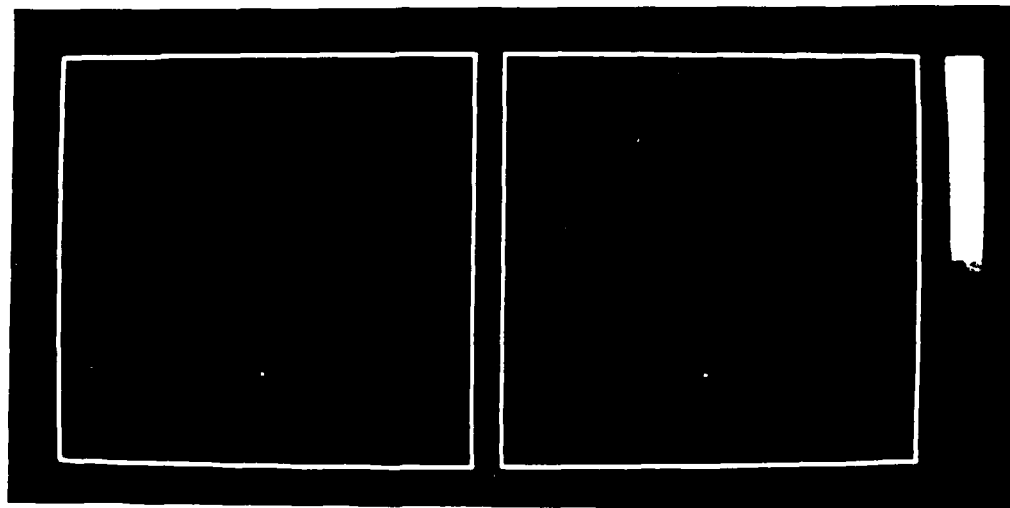
a   b

ISAR Image of a Point Target with
Correlated Random Reflectivity

Figure 4.3

4.3 SIMULATION RESULTS

Several different targets were used for ISAR image generation to observe the effects of correlated random reflectivity and additive noise. First, an image was generated from a point target, located in the center of the field of view, using a correlation interval length of 4.0 pulse intervals, and no added noise. This image is on the left (a) in Figure 4.3. A correlation interval of 4.0 means a correlation time of 0.769 milliseconds. It is seen that the point target is unrecognizable due to the random reflectivity. Also, the image noise is concentrated in the center of the plot. There is a greater time difference between bursts. So, the image is less random in the delay dimension, which is the horizontal in Figure 4.3. The image on the right (b) was generated from the same point target using the same correlation interval including additive noise using an SNR of 10 decibels. It is seen that the added noise has little effect on the image.
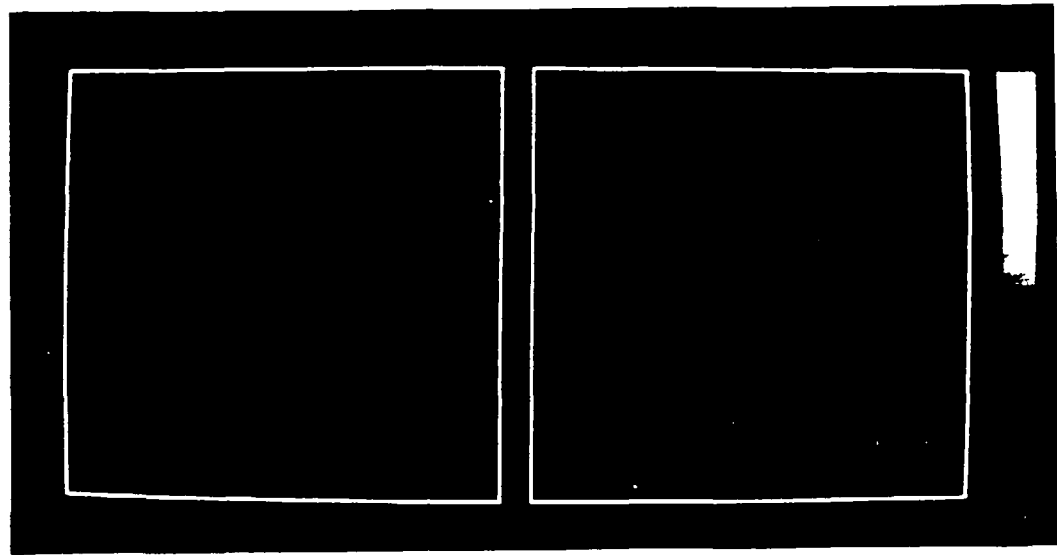
(a)   (b)

ISAR Image of Spherical Target with Random

Reflectivity and Additive Noise

Figure 4.4

For a comparison, an ISAR image was generated from the spherical
target, using correlated random reflectivity of correlation interval 0.5
pulse intervals, and additive noise with SNR of 0 decibels. This image
is shown on the left (a) in Figure 4.4. On the right (b) in the same
picture is an image resulting from processing a mixer signal containing
only additive noise. The result is completely random noise and is
indestinguishable from the sphere's image.

Several images were generated in a parametric study of the effects
of the correlation interval value. A point target in the center of the
image is used. No added noise was put in the mixer output signal. Six
ima   were generated, each with a different value of correlation

interval. The results are displayed in Figure 4.5 with horizontal being
the delay dimension. The correlation interval value increases from
image to image going from top left (a), to top right (c), to lower left
(d), to lower right (f). The noise in the image seems to progressively
narrow horizontally into a vertical line, and then the line shortens
toward a point, as correlation interval increases. The six correlation
interval (CI) values are (a) $CI = 0.5$, (b) $CI = 4$, (c) $CI = 10$, (d) $CI =$
128, (e) $CI = 256$, and (f) $CI = 1100$. The noisy image becomes a line
when the correlation interval equals 128 pulse intervals, the same
length as a burst, the point at which reflectivity is essentially random
only from burst to burst.
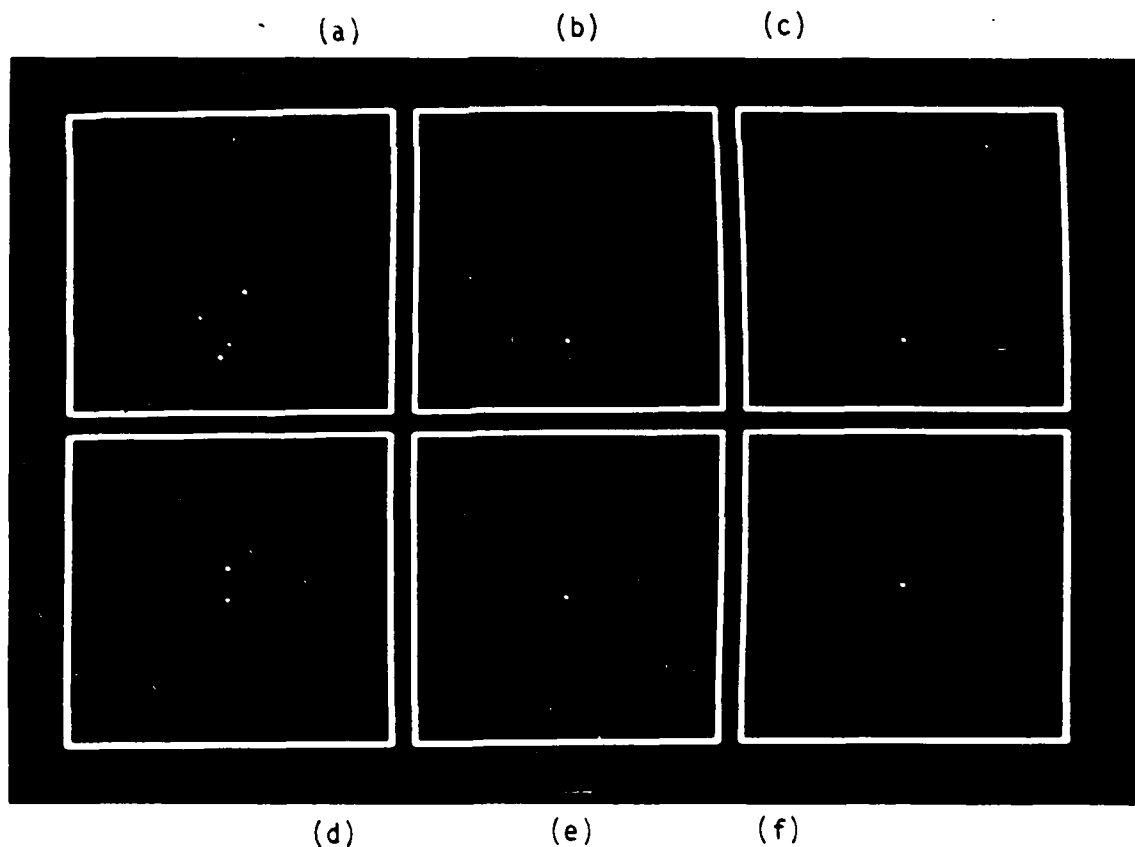
ISAR Images of Point Target Using
Various Correlation Interval Values
Figure 4.5

The simulations presented in Figure 4.5 were repeated using the sphere described previously as the target to be imaged. The results are presented in Figure 4.6. It is seen that as correlation interval increases the target becomes more recognizable.

(a)   (b)   (c)

(d)   (e)   (f)
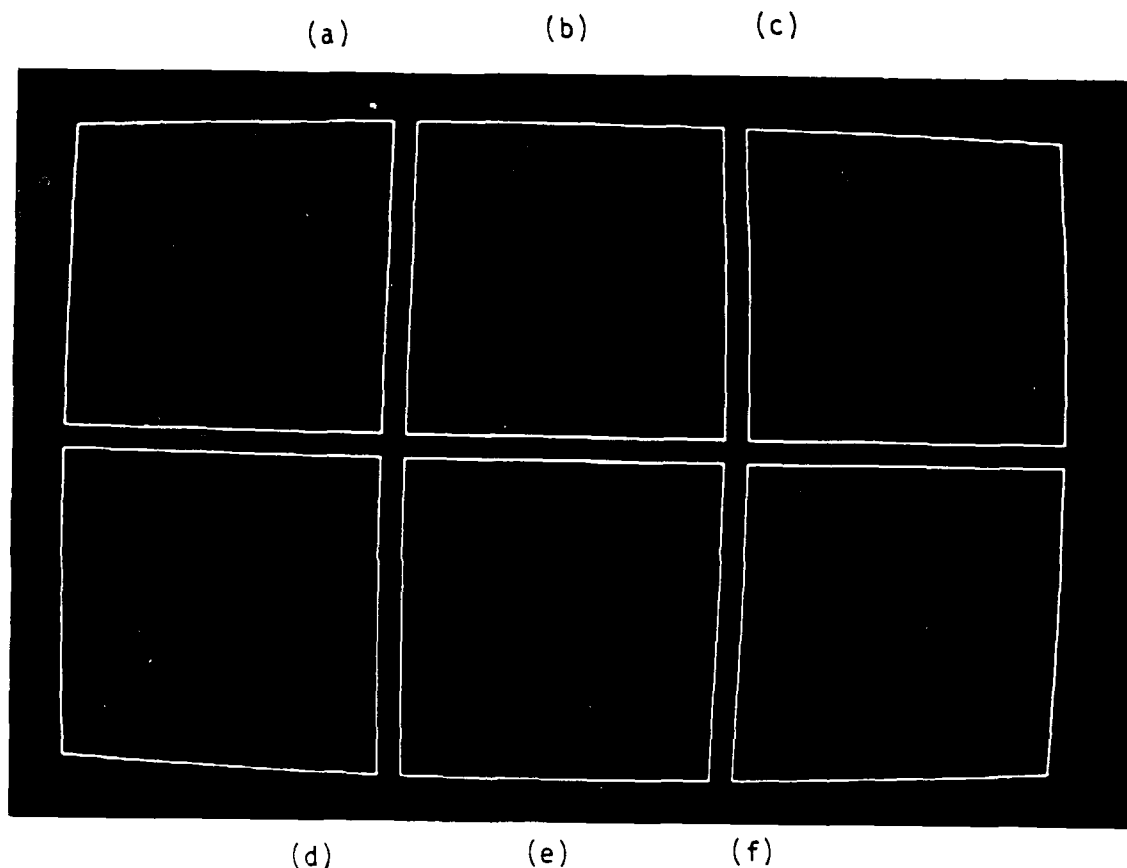
ISAR Images of Spherical Target Using
Various Correlation Interval Values

Figure 4.6

Additionally, examples of windowed ISAR images were generated to see the effects of windowing on diffuse targets and additive noise. On the left (a) in Figure 4.7 is a windowed ISAR image of a center point target having a correlation interval value equal 1100 pulse intervals and no additive noise. Windowing seems to make this point target look like an amorphous blob. The image on the right (b) in the same figure has the same target with additive noise of SNR equal 0.0 decibels added in the signal. The resulting image has additional blurry background. These images suggest that using windowing in generating ISAR images in the presence of noise does not improve image quality.
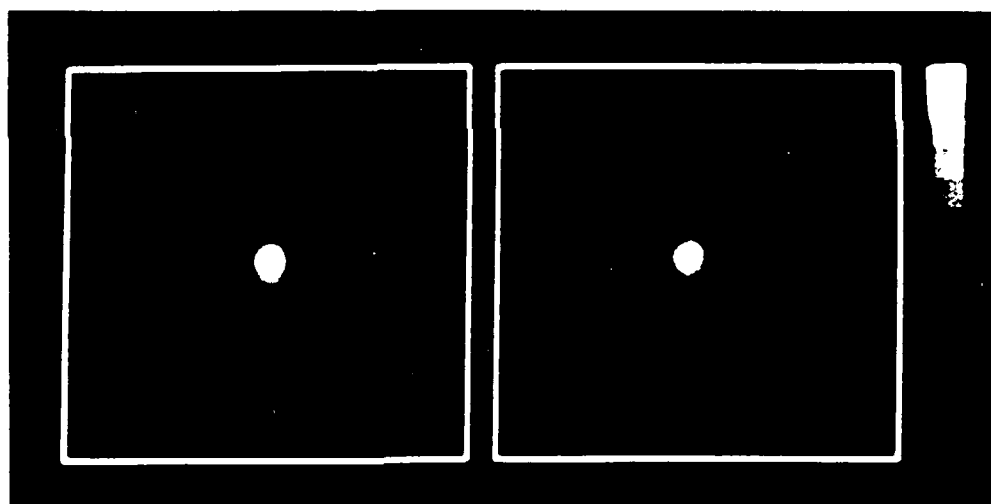
(a)   (b)

Windowed ISAR Images of Center

Point Target

Figure 4.7

4.4 POWER SPECTRUM ESTIMATION

As described before, the mixer output from a diffuse point target, with no added noise, is a temporally correlated random reflectivity multiplied by a delay-doppler signal. In generating an image from this mixer output, Fourier transforms are calculated. The result can be viewed as the convolution of the power density of the target, the desired image, with the Fourier transform of the random reflectivity. The transform squared magnitude of a sequence of random numbers is called a periodogram in (6). Also, this is described as an estimate of the power spectrum of the random process. If the Fourier transform were an unbiased and consistent estimate of the power spectrum, the error in the estimate of the power spectrum would approach zero as the number of samples of the random process gets very large. However, this is not the case. It is shown in (6) that the periodogram is a biased and inconsistent estimate of the power spectrum of a random process. The estimate is biased because the expected value of the periodogram does not equal the power spectrum using limited sample length, and the estimate is inconsistent because the variance of the periodogram does not approach zero as more samples are used in the calculation. This means that ISAR processing as it is conventionally performed cannot accurately reconstruct the power density of of a diffuse target, equivalently the scattering function. An approach for improvement of the power spectrum estimation is the Welch method described in (6). In this method, the data is windowed before the periodogram is computed and several of these smoothed periodograms are averaged. This would require the averaging of several reconstructed images. The Welch method yields a power spectrum

estimate which is biased for limited sample length, though asymptotically unbiased, and the variance of the estimate is expressed as follows.

$$\text{Variance } [B\ (w)] \approx \frac{1}{K}\ P^2(w)\ ,$$

where B is the Welch estimate, K is the number of periodograms averaged, and P is the power spectrum of the random process. The Welch method sacrifices spectral resolution and bias for a consistent spectral estimate. Using the Welch method with limited data probably will not result in a good reconstruction of a scattering function.

5. SUMMARY AND CONCLUSIONS

This thesis work consisted of developing an ISAR imaging simulation using a computer program to input a target scattering function, generate a simulated mixer output signal, and reconstruct an image of the target from the mixer output signal. In the results of Chapter 3, the reflectivity process was fixed at a constant value for each resolution cell, allowing the verification of the ISAR processing since the reconstructed image is expected to look like the scattering function of the target.

With the ISAR simulation verified, the next step reported in Chapter 4 was to implement random reflectivity and additive noise. This was to use the slowly fluctuating target model described in (5). The complex random reflectivity process was correlated in time using a recursive filter. The random reflectivity was kept spatially independent. The results of generating ISAR images using random reflectivity of diffuse targets and additive noise are presented. The reconstructed images show that the random reflectivity has great effect on the image. As a result, the actual target cannot be recognized from the image unless the random reflectivity is highly correlated.

The conclusion is that ISAR processing attempts to measure the power density of the mixer output signal which would look the same as the scattering function, but the random reflectivity makes the calculated power density a random quantity and so the result is a noisy image. Fourier transform techniques yield unsatisfactory results in this application of power spectrum estimation theory.

6. ACKNOWLEDGEMENTS

This thesis was prepared as a part of the radar imaging study project at Washington University, directed by Dr. Donald L. Snyder. I thank Dr. Snyder for the opportunity to work with him on this project and for introducing me to the advanced image reconstruction concepts which were studied.

I want to thank several individuals who helped me during the activities reported in this thesis. Dr. Richard Brueggemann and Dr. Ken Thompson, both of the McDonnell Douglas Corporation, encouraged me greatly during my thesis activities. Trent Wohlschlaeger provided help with using the image processing computer at the University.

7. <u>APPENDIX</u>

APPENDIX 7.1

Program Listings

The listings of the Fortran-77 programs and subroutines used to simulate the mixer output signal and perform ISAR processing to reconstruct an image are included in this appendix. A brief description of each program and subroutine follows.

PROC3, listed in Figure 7.1, calculates a mixer output signal from an input scattering function data file. A non-statistical target is assumed. Subroutine TARGET reads in the scattering function.

VT = Tangential velocity of the target

XFOV, YFOV = Image field of view dimensions

CRX, CRY = location of center of rotation in scattering function

T1 = pulse width (sec)

T3 = Burst length (sec)

W = angular rotation rate in radions per second

BW = bandwidth of burst

FO = lowest frequency (Hz)

FC = center frequency

DF = frequency step size

WL = wavelength

N = number of pulses and bursts

XRES = resolution in meters

RWCF = range walk correction factor

Subroutine IMAGE2D, listed in Figure 7.2, performs ISAR processing to reconstruct an image from radar received signals. The discrete Fourier transforms are implemented using Singleton's Fast Fourier transform algorithm.

PROC4, listed in Figure 7.3, calculates a radar received signal from an input scattering function data file. This routine is a modification of PROC3 to include the effects of a statistical target and additive noise.

CI = correlation interval (# samples) of random reflectivity

SNRDB = signal to noise ratio for additive noise in decibels

Subroutine SCATTER, listed in Figure 7.4, generates components of complex random reflectivity which are correlated in time by recursive filtering white gaussian noise.

Subroutine IMAGE2DW, listed in Figure 7.5, uses data "windowing" as part of the Fourier transform techniques which generate an image.

```
        PROGRAM PROC3
        DIMENSION S(128),Q(128)
        REAL LAMBDA(128,128)
        Complex FRAME(256,256)
        Integer*4 luns
        common /blk1/ luns
C****************************************************************
C*                                                              *
C*       ISAR IMAGING USING A STEPPED-FREQUENCY WAVEFORM        *
C*                                                              *
C*                 BOB LEWIS, DECEMBER 1986                     *
C****************************************************************
        C=3.E8
        C2=2./C
        PI=3.1415927
        PI2=2.*PI
        RES=0.6
        N=128
        YRES=RES
        XRES=RES
        WLCF=0.03
        FC=C/WLCF
        RWC=PI2/YRES/N
        XFOV=N*XRES
        YFOV=N*YRES
        CRX=(N/2-1)*XRES
        CRY=(N/2-1)*YRES
        T1=2.*YFOV/C
        T12=T1/2
        BW=C/(2.*YRES)
        F0=FC-BW/2
        WL=C/F0
        THETA=WL/(2*XRES)
        RANGE=12.5*1852.
        VT=400.*1852./3600.
        W=VT/RANGE
        T3=THETA/(W*N)
        T2=T3/(N-1)
        T4=N*T3
        DF=BW/(N-1)

        CALL fcreat('Enter output filename ',luns)

C****** READ IN THE TARGET'S SCATTERING FUNCTION   ************
        CALL target(LAMBDA)

C****** CALCULATE MIXER OUTPUT SIGNALS AND STORE IN FRAME *****
        L=o5
        DO 100 T=0.,T4,T3
          DO 50 K=1,128
            S(K)=0.
            Q(K)=0.
50        CONTINUE
          DO 30 J=1,128
            X=(J-1)*XRES-CRX
            =.*W
```

PROC3

Figure 7.1

```
          VC2=V*C2
          RWCF=V*T*RWC
          DO 70 I=1,128
             IF(LAMBDA(I,J).EQ.0.)GO TO 70
             A=LAMBDA(I,J)**0.5
             Y=(I-1)*YRES
             DELAY=C2*Y
             DO 60 K=1,128
                K1=K-1
                 FI=K1*DF+F0
                 PHI=PI2*FI*(DELAY-VC2*T)+K1*RWCF
                  S(K)=S(K)+A*COS(PHI)
                  Q(K)=Q(K)+A*SIN(PHI)
   60           CONTINUE
   70        CONTINUE
   80     CONTINUE
          DO 90 K=1,128
            FRAME(K+64,L)=CMPLX(S(K),Q(K))
   90     CONTINUE
          L=L+1
  100 CONTINUE

C****** NORMALIZE MIXER OUTPUT SIGNAL TO PEAK=1.0  **********
      PK=0.
      DO 120 L=1,256
         DO 110 K=1,256
           PK=MAX(PK,ABS(FRAME(L,K)))
  110    CONTINUE
  120 CONTINUE
      PKINV=1./PK
      DO 140 L=1,256
        DO 130 K=1,256
          FRAME(L,K)=FRAME(L,K)*PKINV
  130   CONTINUE
  140 CONTINUE

C****** RECONSTRUCT THE TARGET'S IMAGE ***************
      CALL image2D(FRAME)
      stop
      end
```

PROC3

Figure 7.1 (Continued)

```fortran
      Subroutine  image2D(frame)
      Real image(256,256)
      Complex f(256)
      Complex frame(256,256)
      common /blk1/ luns
C****************************************************
C*                                                 *
C*  This Subroutine reconstructs a radar image     *
C*   by using Fourier transform techniques         *
C*        Bob Lewis. December 1986                 *
C****************************************************

      M=8
C******** DELAY DIMENSION RANGE PROFILES   ***********
      DO 120 j=1,256
        DO 100 i=1,256
          f(i)=conjg(frame(i,j))
100       CONTINUE
        CALL FFT(f,M)
        DO 110 i=1,256
          frame(i,j)=conjg(f(i))*0.0039063
110       CONTINUE
120   CONTINUE

C******** DOPPLER DIMENSION PROFILES        ************
      DO 150 i=1,256
        DO 125 j=1,256
          f(j)=cmplx(0.,0.)
125       CONTINUE
        DO 130 j=1,64
          f(j+64)=frame(i,j+128)
          f(j+128)=frame(i,j+64)
130       CONTINUE
        CALL fft(f,M)
        DO 140 j=1,128
          image(i,j+128)=abs(f(j))**2
          image(i,j)=abs(f(j+128))**2
140       CONTINUE
150   CONTINUE

      nbytes=256*256*4
      CALL fwrite(luns,image,nbytes)
      Return
      END
```

IMAGE 2D

Figure 7.2

```
        PROGRAM PROC4
        REAL LAMBDA(128,128)
        Integer*4 IRAND1,IRAND2
        Complex FRAME(256,256),CNOIS
        Common /blk1/ luns
        Common /blk3/ Y1,Y2,IRAND1,IRAND2
        Dimension GAUSS(2)

C************************************************************************
C*                                                                     *
C*      ISAR WITH CORRELATED COMPLEX RANDOM REFLECTIVITY               *
C*              AND ADDITIVE COMPLEX GAUSSIAN WHITE NOISE              *
C*                      BOB LEWIS, DECEMBER 1986                       *
C************************************************************************
        C=3.E8
        C2=2./C
        PI=3.1415927
        PI2=6.2831854
        RES=0.6
        YRES=RES
        XRES=RES
        N=128
        WL=0.03
        FC=C/WL
        XFOV=N*XRES
        YFOV=N*YRES
        CRX=(N/2-1)*XRES
        CRY=(N/2-1)*YRES
        T1=2.*YFOV/C
        T12=T1/2.
        BW=C/(2.*YRES)
        F0=FC-BW/2
        THETA=2.*ASIN(WL/(4.*XRES))
        RANGE=12.5*1852.
        VT=400.*1852./3600.
        W=VT/RANGE
        T3=THETA/(W*N)
        T2=T3/(N-1)
        T4=N*T3
        DF=BW/(N-1)

        PRINT *,'Input correlation interval'
        READ *,CI

        CALL fcreat('Enter output filename ',luns)

C****** READ IN THE TARGET'S SCATTERING FUNCTION **********
        CALL target(LAMBDA)

        SNRDB=0.0
        IRAND1=322491219
        IRAND2=7
```

PROC4

Figure 7.3

```
C**********************************************************************
C******* SUM TOTAL POWER IN SCATTERING FNC LAMBDA            *******
C**********************************************************************
C******** INITIALIZE 2D ARRAY CONTAINING MIXER OUTPUT SIGNALS *******
C**********************************************************************
      SUMP=0.
      DO 40 I=1,128
          DO 30 J=1,128
              SUMP=SUMP+LAMBDA(I,J)
              FRAME(I+64,J+64)=0.
  30      CONTINUE
  40  CONTINUE


C**********************************************************************
C******** CALCULATE MIXER OUTPUT SIGNALS AND STORE IN FRAME  *******
C********       Loops 90 & 100 change resolution cell        *******
C********       Loop 80 steps burst # , Loop 60 steps pulse # *******
C********       Subroutine SCATTER picks random reflectivity  *******
C**********************************************************************
      DO 100 J=1,128
          X=(J-1)*XRES-CRX
        U=X*W*C2
          DO 90 I=1,128
              IF(LAMBDA(I,J).EQ.0.)GO TO 90
              G=(LAMBDA(I,J)*0.5)**0.5
              Y=(I-1)*YRES
              DELAY=C2*Y
              L=65
              CALL NRMRAN(IRAND1,IRAND2,GAUSS)
              Y1=GAUSS(1)*G
              Y2=GAUSS(2)*G
              DO 80 T=0.,T4,T3
                  DO 60 K=1,128
                      FI=(K-1)*DF+F0
                      PHI=PI2*FI*(DELAY-U*T)
                      CALL SCATTER(G,CI,A,B)
                      S=A*COS(PHI)-B*SIN(PHI)
                      Q=B*COS(PHI)+A*SIN(PHI)
                      FRAME(L,K+64)=FRAME(L,K+64)+CMPLX(S,Q)
  60              CONTINUE
                  L=L+1
  80          CONTINUE
  90      CONTINUE
 100  CONTINUE


C**********************************************************************
C******* Calculate standard deviation of additive noise from SNR *******
C******* Pick additive white Gaussian noise values           *******
C******* Normalize mixer output signal(FRAME) to power=1.0    *******
C******* Add noise to mixer output signal                    *******
C**********************************************************************
      ACS=1./SUMP**0.5
      SNR=10.**(SNRDB/10.)
      ANOIS=1./SNR**0.5
      SDNOIS=ANOIS*0.7071
      DO 120 L=65,192
          DO 110 K=65,192
              CALL NRMRAN(IRAND1,IRAND2,GAUSS)
              SNOIS=GAUSS(1)*SDNOIS
              QNOIS=GAUSS(2)*SDNOIS
              CNOIS=CMPLX(SNOIS,QNOIS)
              FRAME(L,K)=FRAME(L,K)*ACS+CNOIS
 110      CONTINUE
 120  CONTINUE

      CALL image2D(FRAME)
      STOP
      END
```

PROC4

Figure 7.3 (Continued)

```
      subroutine scatter(g,ci,a,b)
C*******************************************************************
C****** This subroutine generates complex random reflectivity  *****
C****** values which are correlated in time by recursive       *****
C****** filtering white Gaussian noise, supplied by NRMRAN.    *****
C******      CI=correlation interval (# samples)               *****
C******          Bob Lewis, Dec. 1986                          *****
C*******************************************************************
      Integer*4 irand1,irand2
      common /blk3/ y1,y2,irand1,irand2
      dimension gauss(2)

      CALL nrmran(irand1,irand2,gauss)
      x1=gauss(1)*g
      x2=gauss(2)*g

      alpha=-1.0/ci
      rho=exp(alpha)
      gamma=(1.-rho**2)**0.5

      y1=rho*y1+gamma*x1
      y2=rho*y2+gamma*x2

      a=y1
      b=y2

      return
      END
```

SCATTER

Figure 7.4

```
      Subroutine image2D(frame)
      Real image(256,256)
      Complex f(256)
      Complex frame(256,256)
      dimension w1(128)
      common /blk1/ luns
C*****************************************************
C*                                                   *
C*   This Subroutine reconstructs a radar image      *
C*   by using windowed Fourier transforms            *
C*            Bob Lewis, December 1986               *
C*****************************************************

      M=8
      sf=5.961
C******** CONSTRUCT WINDOW ***************************
      DO 10 i=1,128
        w1(i)=sf*exp(-0.89*(i-64)**2)
  10    CONTINUE

C******** DELAY DIMENSION RANGE PROFILES   ***********
      DO 120 j=1,256
        DO 100 i=1,256
          f(i)=conjg(frame(i,j))
 100      CONTINUE
        DO 101 i=1,128
          f(i+64)=f(i+64)*w1(i)
 101      CONTINUE
        CALL FFT(f,M)
        DO 110 i=1,256
          frame(i,j)=conjg(f(i))*0.0039063
 110      CONTINUE
 120    CONTINUE

C******** DOPPLER DIMENSION PROFILES       ***********
      DO 150 i=1,256
        DO 125 j=1,256
          f(j)=cmplx(0.,0.)
 125      CONTINUE
        DO 130 j=1,64
          f(j+64)=frame(i,j+128)
          f(j+128)=frame(i,j+64)
 130      CONTINUE
        DO 131 j=1,128
          f(j+64)=f(j+64)*w1(j)
 131      CONTINUE
        CALL fft(f,M)
        DO 140 j=1,128
          image(i,j+128)=abs(f(j))**2
          image(i,j)=abs(f(j+128))**2
 140      CONTINUE
 150    CONTINUE

      nbytes=256*256*4
      CALL fwrite(luns,image,nbytes)
      Return

      END
```

IMAGE 2DW

Figure 7.5

8. BIBLIOGRAPHY

1. D. L. Snyder, H. J. Whitehouse, J. T. Wohlschlaeger, R. C. Lewis, "A New Approach to RADAR/SONAR Imaging," Proceedings of the SPIE 30th Annual Technical Symposium, San Diego, California, August 1986.

2. D. L. Mensa, High Resolution Radar Imaging, Artech House, Inc., Dedham, Massachusetts, 1981.

3. D. Wehner, T. Tice, Wideband Radar, Course Notes, Arizona State University, 1982.

4. A. W. Rihaczek, Principles of High-Resolution Radar, McGraw-Hill, Inc., New York, 1969.

5. H. L. Van Trees, Detection, Estimation, and Modulation Theory, Part III, Radar-Sonar Signal Processing and Gaussian Signals in Noise, John Wiley and Sons, Inc., New York, 1971.

6. A. V. Oppenheim, R. W. Schafer, Digital Signal Processing, Prentice-Hall, Inc., 1975.

7. R. E. Ziemer, W. H. Tranter, Principles of Communications, Houghton Mifflin Company, 1976.

8. M. Schwartz, L. Shaw, Signal Processing: Discrete Spectral Analysis, Detection, and Estimation, McGraw-Hill, Inc., 1975.

9. A. Papoulis, Probability, Random Variables and Stochastic Processes, McGraw-Hill, Inc., 1965, p.465.

9. VITA

Biographical items on the author of the thesis, Mr. Robert C. Lewis.

1) Born June 22, 1955, Memphis, Tennessee.

2) Attended Memphis State University, Memphis, Tennessee. Received the degree of Bachelor of Science in Electrical Engineering in May 1978. Elected chapter President of Tau Beta Pi.

3) Engineer at McDonnell Douglas Corporation, St. Louis, Missouri, May 1978 to present. Has contributed to the research and development in avionics of several advanced aerospace projects including the F-15 fighter and the Tomahawk cruise missile. Author of several government and company reports and outside publications related to these advanced development projects.

4) Attending Washington University, St. Louis, Missouri, September 1982 to present, in the Electrical Engineering department.

May 1987

Short Title: Radar Imaging   Lewis, M. S. 1987

4.2 Copy of Reference 7.

D. L. Snyder, J. A. O'Sullivan, and M. I. Miller, "The Use of Maximum-Likelihood Estimation for Forming Images of Diffuse Radar-Targets from Delay-Doppler Data," Tech. Rpt. Electronic Systems and Signals Research Laboratory, Washington University, St. Louis, May 1987.

THE USE OF MAXIMUM-LIKELIHOOD ESTIMATION FOR FORMING IMAGES OF DIFFUSE RADAR-TARGETS FROM DELAY-DOPPLER DATA†

Donald L. Snyder
Joseph A. O'Sullivan
and
Michael I. Miller

Electronic Systems and Signals Research Laboratory
Department of Electrical Engineering
Washington University
St. Louis, MO 63130

ABSTRACT

The expectation-maximization algorithm for computing maximum-likelihood estimates iteratively is used to develop a new approach for processing inverse synthetic-aperture radar data to form images of fluctuating, diffuse radar-targets. The scattering function of the target is imaged by jointly estimating the power spectra of wide-sense stationary reflectivity-processes occurring in all the range cells that span the target. The complex-valued reflectivity processes are also estimated. The results we obtain apply to imaging-radar systems operating at radio and optical frequencies when target echos have no specular or glint components.

1. Introduction

An inverse synthetic-aperture radar (ISAR) system is used to form an image of a radar target. This is accomplished by illuminating the target with a series of pulses and observing the return echos. Each patch on the target introduces a certain amount of propagation delay and doppler shift to a pulse it reflects, the amount depending on the range and range rate of the patch relative to the radar system. The received signal for each illumination is a complicated superposition of the reflections from all patches that make up the extended surface of the target. The goal in processing the received signal is to produce an image of the target.

The design of an ISAR system includes the selection of the transmitted waveform, the selection of a model for the reflection process by which a portion of the transmitted waveform is returned to the receiver, and the selection of the algorithm used to process the received waveform to create the target's image. The beam-width of the radar antenna relative to the size of the target is also a design consideration; images can be produced by either scanning a narrowly focused beam over the target in some type of raster pattern or by illuminating the entire target in *spotlight mode* with a wide, relatively unfocused beam. Our concern will be with forming images of rotating, rough targets using a spotlight-mode radar.

Stepped-frequency and *linear-FM chirp* are two modulation formats used with transmitted pulse-sequences in spotlight-mode radar-imaging. Stepped-frequency pulses are described by Prickett, Wehner, and Chen [1], Ruttenberg and Chanzit [2], and Chen and Andrews [3]. The target is illuminated with a sequence of N pulse-groups, where each group is identical and is formed from a sequence of N narrow pulses having equal incremental steps in frequency. The usual approach for processing delay- and doppler-shifted echos acquired by illuminating a rotating target with this waveform consists of two steps. The first is to place the data, consisting of one sample-value per transmitted pulse, into delay (or, range) bins by separately Fourier transforming the N sample values from each pulse group. The resulting delay-binned data are placed in the rows of an $N \times N$ matrix, where each row contains the transformed data from one pulse-group. In the second step, the columns of this matrix are Fourier transformed to obtain a doppler (or, cross-range) profile at each delay. The resulting two-dimensional array is intended to be the target's complex-valued reflectance function in delay (range) and doppler (cross-range) coordinates, the magnitude or squared magnitude of which can be displayed as the

target's image. This processing based on two-dimensional Fourier transforms is derived using a deterministic analysis that does not account for statistical properties of the reflectivity or any noise that may be present.

Wideband "chirp" pulses, having an instantaneous frequency that varies linearly with time, are also used for radar imaging. The common approach is to transmit a series of pulses, each of which has an identical envelope and chirp rate. A variety of processing approaches are described in the literature, including two-dimensional Fourier transformation by Mensa [4] and Walker [5] and tomographic reconstruction by Mensa [4] and Munson, O'Brian, and Jenkins [6]. A variant of the stepped-frequency format in which each narrow pulse in a pulse group is a chirp is described by Blahut [7]

Bernfeld [8] introduced the concept of using chirp-rate modulation with processing based on tomographic reconstructions to image the target's scattering function for radar signals having a large time-bandwidth product. With his approach, the target is illuminated by a sequence of linear-FM chirped pulses, with each pulse having a distinct chirp rate. Bernfeld notes that the output of a matched-filter receiver for a radar waveform with an infinite time-bandwidth product is a line integral through the scattering function, where the angular orientation of the line of integration for a pulse is a function of the chirp rate of that pulse. This observation suggests using the same algorithms as used in x-ray tomography to determine the scattering function. Snyder, Whitehouse, Wohlschlaeger, and Lewis [9] extended Bernfeld's approach to include waveforms with more modest time-bandwidth products. This is accomplished by noting similarities to the tomographic imaging of radioactive tracers, where ideal line-integrals are not available.

The approach we describe in this paper can accommodate the stepped-frequency and chirp formats as well as others. It represents a continuation of our examination of how the approaches currently used in emission tomography can be applied to radar imaging. The method we have described in [9] is adapted from the best algorithm for time-of-flight emission tomography when the processing of the data is required to be linear [10]. A more fundamental approach described by Snyder and Politte [11] leads to nonlinear processing and improved accuracy in forming images of radioactivity distributions. In this paper, we describe the initial

results we have obtained in adopting an analogous approach for radar imaging. This relies on the use of a mathematical model for data acquired in a spotlight-mode radar and on the use of the method of maximum-likelihood estimation.

Van Trees [12] and Shapiro, Capron, and Harney [13] describe models for fluctuating, diffuse radar-targets. The models are based on the assumption that the surface of the target is rough compared to the wavelength of the radar illumination. The reflectance is modeled as a Gaussian wide-sense stationary, uncorrelated scatter (WSSUS) process, which is uncorrelated in range and temporally stationary. Such models are accurate for some targets in radio- and optical-frequency radar-imaging systems; but not all. An important effect not included in our present results is that of glint or specular components in radar returns. We are currently attempting to extend our approach to include these additional effects.

Model based approaches that use statistical estimation-theory techniques appear less frequently in the large literature of radar imaging. One example is that of Frost, Stiles, Shanmugan, and Holtzman [14], who use a multiplicative model and Wiener-filtering techniques. Our approach differs in that the model we adopt for the return signal is more complicated than a simple multiplicative one and depends explicitly on the transmitted waveform through a spatial integration over the target. We also do not restrict the processing to be linear; in particular, we show that the processing of the received data for producing the maximum-likelihood estimate of the target's scattering function is not linear.

Radar imaging systems generally produce estimates of one or the other of two quantities that can be viewed as the target's image. Some approaches produce an estimate of the target's complex-valued reflectivity as a function of range and cross range, while others produce an estimate of the target's scattering function. For the new approach we describe, the reflectivity process is modeled as a complex-valued Gaussian random-process that is temporally stationary and spatially white. The scattering function is the power-density spectrum of this process as a function of delay. We treat both the reflectivity process and its second-order statistic, the scattering function, as unknown quantities. The iterative approach we develop yields the maximum-likelihood estimate of the scattering function and, simultaneously, the conditional-mean estimate of the reflectivity based on statistics which are consistent with the estimated

scattering-function. Thus, both of the quantities treated separately in other imaging schemes are produced simultaneously with our new approach. This is unique to our approach, and we feel that it is important.

We will develop a necessary condition, called the *trace condition*, which the maximum-likelihood estimate of the target's scattering function must satisfy. This equation appears to be very hard to solve directly. As a consequence, we reformulate the imaging problem using the concept of incomplete-complete data spaces and then use the expectation-maximization algorithm to derive an iterative algorithm for producing the maximum-likelihood estimate of the scattering function. This procedure also yields the conditional-mean estimate of the reflectance. The technique we use to accomplish this parallels that described by Miller and Snyder in [15] for power-spectrum estimation and extends their results to include indirect measurements of the process whose spectrum is desired; the process is now measured following a linear transformation and in additive noise. As shown by Turmon and Miller [16], this approach to spectrum estimation results in estimated spectra with less bias and mean-square error than other approaches discussed in the literature. We expect similar improvements will be seen in radar imaging of scintillating, diffuse targets when this new technique is used.

2. Model

The model and notation we shall use closely follows that of Van Trees [12, Ch. 13]. The complex envelope of the transmitted signal will be denoted by $2E_T^{1/2}s_T(t)$ where E_T is the transmitted energy and $s_T(t)$ is normalized to unit energy. Thus, the transmitted signal is given by

$$\sqrt{2E_T}\,\text{Re}[s_T(t)\exp(j2\pi f_0 t)], \tag{1}$$

where f_0 is the carrier frequency of the radar. For a stepped-frequency waveform consisting of N pulse groups with N pulses in each group, the complex envelope is given by

$$s_T(t) = \sum_{i=0}^{N-1} \sum_{n=0}^{N-1} p(t - nT_p - iT_g)\exp(j2\pi\Delta_n(t - nT_p - iT_g)), \tag{2}$$

where T_p and T_g denote the time interval between pulses in a group and between groups, respectively, Δ_n is the increment to the carrier frequency f_0 of the n-th pulse in a group, and $p(t)$ is the complex envelope of a pulse. For pulses typically assumed, the envelope $|p(t)|$ is a narrow, rectangular function, and the phase $\arg[p(t)]$ is zero. For a sequence of N pulses having chirp-rate modulation,

$$s_T(t) = \sum_{i=0}^{N-1} p(t - iT_p)\exp\left(j\pi\beta_i(t - iT_p)^2\right), \tag{3}$$

where β_i is the chirp rate of the i-th pulse, and iT_p is its delay.

Patches on the target with a two-way delay in the interval $[\tau, \tau + \Delta\tau)$ reflect a signal that is incident on the patch at time t with strength $b(t,\tau)\Delta\tau$. Consequently, the complex envelope of the received signal $s_R(t)$ following the illumination of the target by $s_T(t)$ is given by the following superposition of returns from reflecting patches at all the two-way delays τ.

$$s_R(t) = \sqrt{2E_T} \int_{-\infty}^{\infty} s_T(t - \tau)b\left(t - \frac{1}{2}\tau, \tau\right)d\tau. \tag{4}$$

Van Trees [12] and Shapiro, Capron, and Harney [13] discuss the reflectance process $b(t,\tau)$ for targets that are rough compared to the wavelength at the carrier of radio- and

optical-frequency radar-systems. For such diffuse targets, without any glint components in the return signal, $b(t,\tau)$ may be taken to be a complex-valued Gaussian random-process with zero mean and covariance

$$E[b(t,\tau)b^*(t',\tau')] = K(t-t',\tau)\delta(\tau-\tau'), \tag{5}$$

where "*" denotes complex conjugation, the impulse function in delay results because of the assumption of uncorrelated scattering, and $K(t,\tau)$ is the covariance function of the reflectance at each delay τ. The Fourier transform of $K(t,\tau)$ with respect to t is the scattering function $S(f,\tau)$ of the target,

$$S(f,\tau) = \int_{-\infty}^{\infty} K(t,\tau)\exp(-j2\pi ft)dt. \tag{6}$$

This is the power-density spectrum of the reflectance process for all scattering patches at delay τ.

We will model the complex envelope of the total return signal $r(t)$ as

$$r(t) = s_R(t) + w(t), \tag{7}$$

where $w(t)$ is complex-valued Gaussian white noise that is uncorrelated with the reflectance process. The mean of $w(t)$ is zero, and the covariance is

$$E[w(t)w^*(t')] = N_0\delta(t-t'). \tag{8}$$

The scattering function $S(f,\tau)$ of a diffuse, rotating radar target provides an image of the target in doppler (or cross range) and delay (or range) coordinates. $S(f,\tau)\Delta f\Delta\tau$ is the mean-square strength (or power) of the reflectance of all patches on the target having a doppler shift in the interval $[f,f+\Delta f)$ and a delay in the interval $[\tau,\tau+\Delta\tau)$. We may, therefore, state the problem of imaging a diffuse radar-target as that of estimating the scattering function $S(f,\tau)$ or, equivalently, the covariance function $K(t,\tau)$ given radar-return data $\{r(t), T_i \leq t \leq T_f\}$ on an observation interval (T_i,T_f).

discrete model

In anticipation of using discrete-time processing of radar data to produce images, we now state the discrete version of our model as follows. We are given N samples of the complex-valued radar-data corresponding to (7),

$$r(n) = s_R(n) + w(n), \qquad n = 0, 1, \dots, N-1,$$ (9)

where $w(n)$ is a white Gaussian-sequence with zero mean and covariance

$$E[w(n)w^*(n')] = N_0 \delta_{n,n'},$$ (10)

and where the signal samples corresponding to (4) are given by

$$s_R(n) = \sqrt{2E_T} \sum_{i=-\infty}^{\infty} s_T(n,i)b(n,i), \qquad n = 0, 1, \dots, N-1.$$ (11)

In this expression, we define $s_T(n,i)$ and $b(n,i)$ in terms of the transmitted signal and the reflectance process, respectively, according to:

$$s_T(n,i) = s_T(n\Delta t - i\Delta\tau),$$ (12)

and

$$b(n,i) = b\left(n\Delta t - \frac{1}{2}i\Delta\tau, i\Delta\tau\right)\Delta\tau,$$ (13)

where Δt and $\Delta\tau$ are the sampling intervals adopted in the discretization in time and delay, respectively. We assume that the target has a finite extent, so $b(n,i)$ and, therefore also, terms forming the sum in (11) are zero for i outside the I values $m, m+1, \dots, m+I-1$ starting from the minimum two-way delay corresponding to m. This discrete reflectance is a Gaussian sequence with zero mean and covariance given by

$$E[b(n,i)b^*(n',i')] = K(n - n', i)\delta_{i,i'}.$$ (14)

The discrete scattering function $S(f,i)$ is the Fourier transform of $K(n,i)$,

- 7 -

$$S(f,i) = \sum_{n=-\infty}^{\infty} K(n,i)\exp(-j2\pi fn).$$ (15)

The imaging problem for the discrete model is to estimate $S(f,i)$, or equivalently the covariance function $K(n,i)$, for all frequencies f spanning the target in doppler, and for all delays i spanning the target in delay, given the radar data $(r(n), n=0, 1, ..., N-1)$.

matrix model

These discrete equations may conveniently be written in matrix form as follows. Define r to be the received-signal vector of dimension N,

$$r = \begin{pmatrix} r(0) \\ r(1) \\ \cdot \\ \cdot \\ \cdot \\ r(N-1) \end{pmatrix} = s_R + w,$$ (16)

where the N-dimensional vectors, s_R and w, are given by

$$s_R = \begin{pmatrix} s_R(0) \\ s_R(1) \\ \cdot \\ \cdot \\ s_R(N-1) \end{pmatrix} \quad \text{and} \quad w = \begin{pmatrix} w(0) \\ w(1) \\ \cdot \\ \cdot \\ w(N-1) \end{pmatrix}.$$ (17)

Also, define S^* as the $NI\times N$ rectangular matrix expressed in column-block form in terms of I separate $N\times N$ matrices according to

$$S^* = \begin{pmatrix} S_0 \\ S_1 \\ \cdot \\ \cdot \\ \cdot \\ S_{I-1} \end{pmatrix},$$ (18)

where S_i is an $N\times N$ diagonal matrix containing sample values of the complex envelope of the transmitted signal $s_T(t)$,

$$S_j = \begin{pmatrix} s_T(0,m+j) & 0 & 0 & \cdot & \cdot & 0 \\ 0 & s_T(1,m+j) & 0 & \cdot & \cdot & 0 \\ 0 & 0 & \cdot & \cdot & \cdot & 0 \\ \cdot & & \cdot & \cdot & \cdot & \cdot \\ 0 & 0 & \cdot & \cdot & \cdot & s_T(N-1,m+j) \end{pmatrix}. \tag{19}$$

Further, define the reflectance vector b of dimension NI in the column-block form of I vectors according to

$$b = \begin{pmatrix} b(0) \\ b(1) \\ \cdot \\ \cdot \\ \cdot \\ b(I-1) \end{pmatrix}, \tag{20}$$

where each $b(i)$ is a vector of dimension N,

$$b(i) = \begin{pmatrix} b(0,m+i) \\ b(1,m+i) \\ \cdot \\ \cdot \\ \cdot \\ b(N-1,m+i) \end{pmatrix}. \tag{21}$$

Using (11) and these definitions, we can now express the N-dimensional signal vector s_R of (15) and (16) as

$$s_R = \sqrt{2E_T}\, S^+ b, \tag{22}$$

where "+" denotes an Hermitian transpose. In terms of these defined matrices, the received vector has zero mean and covariance

$$K_r = E(rr^+) = E(s_R s_R^+) + E(ww^+)$$
$$= 2E_T S^+ E(bb^+) S + N_0 I. \tag{23}$$

Then, since

$$E(b(i)b^+(j)) = K(i)\delta_{i,j}, \tag{24}$$

where $K(i)$ is the Hermitian-symmetric Toeplitz-matrix

$$K(i) = \begin{pmatrix} K(0,m+i) & K*(1,m+i) & \cdot & \cdot & K*(N-1,m+i) \\ K(1,m+i) & K(0,m+i) & \cdot & \cdot & \cdot \\ \cdot & \cdot & \cdot & \cdot & \cdot \\ K(N-1,m+i) & & \cdot & \cdot & K(0,m+i) \end{pmatrix},$$ (25)

it follows from (23) that the covariance K_r of r is given by

$$K_r = 2E_T S^* K S + N_0 I,$$ (26)

where K is the block-diagonal $NI \times NI$ dimensional matrix defined by

$$K = \begin{pmatrix} K(0) & 0 & 0 & \cdot & \cdot & 0 \\ 0 & K(1) & 0 & \cdot & \cdot & 0 \\ \cdot & \cdot & \cdot & \cdot & \cdot & \cdot \\ 0 & 0 & 0 & \cdot & \cdot & K(I-1) \end{pmatrix}.$$ (27)

The i-*th* diagonal block $K(i)$ of K is the covariance matrix of the reflectance process at the i-*th* delay bin. The imaging problem in terms of these expressions is, then, to estimate the matrix K of (27) given the data vector r of (16). The scattering function then can be determined from K by using (15).

3. Maximum-Likelihood Imaging for the Incomplete-Data Model

For reasons that will become evident in the next section, we term the N-dimensional data vector r the *incomplete data* for the radar-imaging problem. The model given in the last section for this incomplete data is that r is normally distributed with zero mean and covariance specified in (26). Given the incomplete data, we wish to estimate the covariance K of the reflectance process, as defined in (27). To do this, we adopt the maximum-likelihood method of statistics, which selects K to maximize the incomplete-data loglikelihood

$$L_{id}(K) = -\frac{1}{2}\ln\big(\det\big(2E_T S^* K S + N_0 I\big)\big) - \frac{1}{2}r^*\big(2E_T S^* K S + N_0 I\big)^{-1} r,$$

(28)

where the maximization is subject to the constraint that K be an admissible matrix, where by an *admissible matrix* we mean a matrix having the block-diagonal form in (27) with each diagonal block being a Hermitian-symmetric, positive-semidefinite Toeplitz-matrix.

We now derive a necessary condition, termed the *trace condition*, which the matrix maximizer of the incomplete-data loglikelihood (28) must satisfy. In principle, this equation specifies the maximum-likelihood estimate of K. If K maximizes $L_{id}(K)$ of (28), then $L_{id}(K+\delta K) < L_{id}(K)$ for δK small. Equivalently, the first derivative is zero,

$$\lim_{\alpha \to 0} \frac{L_{id}(K + \alpha \delta K) - L_{id}(K)}{|\alpha|} = 0,$$

(29)

for all matrix variations δK with α real such that $K + \alpha \delta K$ is admissible. As shown in the Appendix, this implies the trace condition,

$$\mathrm{Tr}\Big(\big(2E_T S^* K S + N_0 I\big)^{-1}\big(rr^* - 2E_T S^* K S - N_0 I\big)\big(2E_T S^* K S + N_0 I\big)^{-1} S^* \delta K S\Big) = 0,$$

(30)

which must be satisfied by the maximum-likelihood estimate K. Burg, Luenberger, and Wenger [17] have studied an equivalent problem of Toeplitz-constrained covariance-estimation and have derived the trace condition using a different approach.

There are NI unknowns in K. Since δK must be a block diagonal matrix of Hermitian-symmetric Toeplitz-matrices, there are NI parameters in δK that can be varied. These variations in the trace condition (30) generate NI equations in the unknown elements of K. Thus, in principle, the trace condition produces enough equations to determine the

maximum-likelihood estimate K. However, the equations are complicated due to the inverse matrices appearing in (30), so it does not appear to be feasible to determine K directly from the trace condition, which motivates our development of the iterative approach in the next section. The trace condition is only a necessary condition which the estimate K must satisfy. For it to be sufficient as well, the second derivative must be negative along all admissible variational directions δK. In the Appendix, an expression for the second derivative in the direction δK is obtained.

In the next section, we will develop an iterative procedure for determining a sequence of estimates that increase the likelihood at each iteration stage. We will demonstrate that the limit point of the iterations satisfies the trace condition (30).

4. Maximum-Likelihood Imaging for the Incomplete/Complete Data Model

That the trace condition (30) cannot be solved directly for the maximum-likelihood estimate of K motivates the indirect approach we now take of embedding the imaging problem in a larger, seemingly more difficult problem. The result will be an iterative algorithm which when implemented produces a sequence of admissible matrices $K^{(0)}$, $K^{(1)}$, ..., $K^{(k)}$, ... having the property that the corresponding sequence of incomplete-data loglikelihoods $L_{id}[K^{(0)}]$, $L_{id}[K^{(1)}]$, ..., $L_{id}[K^{(k)}]$, ... is nondecreasing at each stage.

Fuhrmann and Miller [18] have recently shown that maximum-likelihood estimates of Toeplitz-constrained covariances which are positive definite do not always exist when given only one data vector r. A necessary and sufficient condition for the likelihood function to be unbounded, and therefore for no maximum-likelihood estimate to exist, is that there be a singular Toeplitz matrix with the data in its range space. For our imaging problem, this condition is that there exists an admissible K with

$$2E_T S^* KS + N_0 I$$

singular such that

$$r = \left(2E_T S^* KS + N_0 I\right)\alpha$$

for some complex-valued vector α. In fact, without constraining K further than being Toeplitz, a sufficient condition that a singular estimate for K be obtained is that $N_0 = 0$ and there exists a singular K with r in the range space of $2E_T S^+ KS$. The argument for this mirrors that of Fuhrmann and Miller in [18, Theorem 1], but is applied to the complete data loglikelihood (35). Furhmann and Miller also showed that even if the true covariance had eigenvalues bounded from above and below, the probability that there exists a singular Toeplitz matrix with the data in its range can be very close to one. By restricting the search to Toeplitz matrices with circulant extensions, they were able to show that the probability a singular circulant Toeplitz matrix has the data in its range space is zero. Thus, in order for maximum-likelihood estimates to be nonsingular with probability one for all nonnegative values of N_0, we restrict the class of admissible Toeplitz matrices to be those with circulant extensions of period P, where P is equal to or greater than the number N of data samples available, $P \geq N$. What we envision in adopting this constraint is that for each delay i, the N sample values of the reflectance $b(n,i)$, n

= 0, 1, ..., N-1, are from a stationary process that is periodic with period P, where P could be some large but finite value. These N sample values enter the incomplete data r according to (15) and (22). By using the expectation-maximization algorithm of Dempster, Laird, and Rubin [19], we shall develop a sequence of admissible matrices that have the maximum-likelihood estimate of K subject to this circulant extension as a limit point. The approach parallels that of Miller and Snyder [15] for estimating the power spectrum of a time-series from a single set of data. An important benefit of introducing the periodic extension and using the expectation-maximization algorithm is that estimates of both the scattering function and the reflectance process are obtained simultaneously and can be readily viewed as target images in range and cross-range coordinates; thus, the procedure proposed may be considered to be natural for the imaging problem because both types of images considered separately in the past are obtained directly. For completeness, we also include in the Appendix the equations obtained using the expectation-maximization algorithm for estimating general Toeplitz matrices when the assumption of a circulant extension is not made.

We shall introduce a modification of our notation to indicate that the N samples of the reflectance process are from a stationary periodic-process of period P. Thus, let $b_N(i)$ denote the N-dimensional vector $b(i)$ of (21). We now think of $b_N(i)$ as an N-dimensional subvector of the P-dimensional vector $b_P(i)$ formed from samples of the reflectance process over a full period,

$$b_P(i) = \begin{pmatrix} b(0, m+i) \\ b(1, m+i) \\ \cdot \\ \cdot \\ b(N-1, m+i) \\ \cdot \\ \cdot \\ b(P-1, m+i) \end{pmatrix}. \tag{31}$$

If I_N is the N×N identity matrix, and if J is the P×N matrix defined by

$$J = \begin{pmatrix} I_N \\ 0 \end{pmatrix}, \tag{32}$$

then $b_N(i) = J^+ b_P(i)$. Also, let b_N denote the NI-dimensional vector b of (20), and let b_P be the PI-dimensional vector with i-*th* block element $b_P(i)$. Then, $b_N = M^+ b_P$, where M is the $PI \times NI$ block diagonal-matrix

$$M = \begin{pmatrix} J & 0 & 0 & \cdot & \cdot & 0 \\ 0 & J & 0 & \cdot & \cdot & 0 \\ \cdot & \cdot & \cdot & \cdot & \cdot & \cdot \\ 0 & 0 & 0 & \cdot & \cdot & J \end{pmatrix}. \tag{33}$$

Furthermore, let $K_N(i)$ denote the $N \times N$ Toeplitz covariance-matrix $K(i)$ of $b_N(i)$ defined in (25), and let $K_P(i)$ denote the $P \times P$ circulant covariance-matrix of $b_P(i)$. Then, the Toeplitz matrix $K_N(i)$ is the upper left block of the circulant matrix $K_P(i)$, as given by

$$K_N = J^* K_P(i) J.$$

Lastly, let K_P denote the $PI \times PI$ block-diagonal matrix in the form of (27) with the i-*th* diagonal block being $K_P(i)$. Then, if K_N denotes the $NI \times NI$ matrix K of (27), there holds

$$K_N = M^* K_P M.$$

For use with the expectation-maximization algorithm, we identify the *complete data* as (b_P, w), where w is the N-dimensional noise vector defined in (16). We note from (15), (22), and the above definitions that the incomplete data r can be obtained from the complete data according to the mapping

$$r = \sqrt{2E_T} S^* M^* b_P + w. \tag{34}$$

The loglikelihood function $L_{cd}(K_P)$ of the complete data is given by

$$L_{cd}(K_P) = -\frac{1}{2} \ln(\det(K_P)) - \frac{1}{2} b_P^* K_P^{-1} b_P, \tag{35}$$

where all terms that are not a function of K_P have been suppressed.

Let W denote the $P \times P$ discrete Fourier-transform matrix scaled so that the columns are orthonormal,

$$W = \frac{1}{\sqrt{P}} \begin{pmatrix} w_P^0 & w_P^0 & \cdot & \cdot & w_P^0 \\ \cdot & \cdot & \cdot & \cdot & \cdot \\ w_P^0 & w_P^k & w_P^{2k} & \cdot & w_P^{(P-1)k} \\ \cdot & \cdot & \cdot & \cdot & \cdot \\ w_P^0 & w_P^{P-1} & \cdot & \cdot & w_P^{(P-1)(P-1)} \end{pmatrix}, \tag{36}$$

where $w_P = \exp(-j2\pi/P)$. Also, let W_P be the $PI \times PI$ block-diagonal matrix

$$W_P = \begin{pmatrix} W & 0 & 0 & \cdot & \cdot & 0 \\ 0 & W & 0 & \cdot & \cdot & 0 \\ \cdot & \cdot & \cdot & \cdot & \cdot & \cdot \\ 0 & 0 & 0 & \cdot & \cdot & W \end{pmatrix}. \tag{37}$$

Then, b_P can be represented in rotated coordinates according to

$$c_P = W_P b_P = \begin{pmatrix} c(0) \\ c(1) \\ \cdot \\ \cdot \\ c(I-1) \end{pmatrix}, \tag{38}$$

where $c(i) = Wb_P(i)$. The assumption that $b_P(i)$ originates from a periodic process implies that the PI-dimensional vector c_P is normally distributed with zero mean and diagonalized covariance

$$\Sigma_P = E(c_P c_P^*) = W_P K_P W_P^*. \tag{39}$$

We will denote the $(p+iI)$-*th* diagonal element of Σ_P by $\sigma_p^2(i)$; this is the p-*th* diagonal element of the $P \times P$ diagonal matrix $E[c(i)c^+(i)]$.

Substituting the expression

$$K_P = W_P^* \Sigma_P W_P \tag{40}$$

into (35) indicates that the complete-data loglikelihood can alternatively be expressed as a function of Σ_P according to
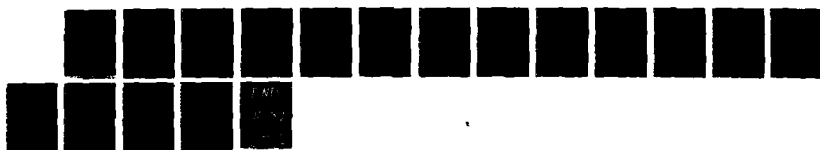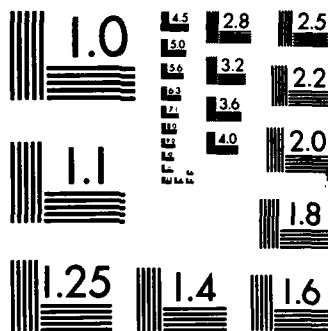
MICROCOPY RESOLUTION TEST CHART
NATIONAL BUREAU OF STANDARDS-1963-A

$$L_{cd}(\Sigma_P) = -\frac{1}{2}\ln(\det(\Sigma_P)) - \frac{1}{2}c_P^*\Sigma_P^{-1}c_P$$

$$= -\sum_{i=0}^{I-1}\sum_{p=0}^{P-1}\ln(\sigma_p(i)) - \frac{1}{2}\sum_{i=0}^{I-1}\sum_{p=0}^{P-1}|c_p(i)|^2\sigma_p^{-2}(i), \tag{41}$$

where $c_p(i)$ is the p-*th* element of the *P*-dimensional vector $c_P(i)$.

The expectation-maximization algorithm for estimating the covariance of the reflectance process K_P from the incomplete data r is an alternating maximization procedure in which a sequence of estimates of Σ_P having increasing likelihood is obtained first. If $\Sigma_P(k)$ denotes the estimate of Σ_P at stage k, then there is a corresponding element, $K_P(k) = W_P^+\Sigma_P(k)W_P$ in a sequence of estimates of K_P having increasing likelihood. Likewise, to the k-*th* element $K_P(k)$ of the sequence of estimates of K_P, there is a corresponding element, $K_N(k) = M^+K_P(k)M$, in a sequence of estimates of K_N having increasing likelihood.

Each iteration stage of the expectation-maximization algorithm has an expectation (E) step and a maximization (M) step that must be performed to get to the next step. The E-step requires evaluation of the conditional expectation of the complete-data loglikelihood (41) given the incomplete data r and assuming that the covariance defining the complete data is $\Sigma_P(k)$,

$$Q[\Sigma_P|\Sigma_P^{(k)}] = E[L_{cd}(\Sigma_P)|r,\Sigma_P^{(k)}]. \tag{42}$$

From (41), we have that

$$Q[\Sigma_P|\Sigma_P^{(k)}] = -\sum_{i=0}^{I-1}\sum_{p=0}^{P-1}\ln(\sigma_p(i)) - \frac{1}{2}\sum_{i=0}^{I-1}\sum_{p=0}^{P-1}E[|c_p(i)|^2|r,\Sigma_P^{(k)}]\sigma_p^{-2}(i). \tag{43}$$

The M-step yields the estimate $\Sigma_P(k+1)$ at stage $k+1$ as the choice of Σ_P that maximizes this conditional expectation,

$$\Sigma_P^{(k+1)} = \arg\max[Q(\Sigma_P|\Sigma_P^{(k)})], \tag{44}$$

subject to the constraint that the maximizer be a diagonal covariance-matrix. From (43), this maximization yields the diagonal matrix $\Sigma_P(k+1)$ with (p+iI)-*th* diagonal element

$$(\sigma_p^2(i))^{(k+1)} = E[|c_p(i)|^2|r,\Sigma_P^{(k)}]. \tag{45}$$

Thus, we may write $\Sigma_P^{(k+1)}$ as

$$\Sigma_P^{(k+1)} \stackrel{d}{=} E[\, c_P c_P^* \,|\, r , \Sigma_P^{(k)} \,],$$ (46)

where the "d" over the equal sign means that the diagonal terms in the matrix on the left side equal the diagonal terms in the matrix on the right side and that all the off diagonal elements on the left side are zero.

The above expression (46) appears to be complicated because of the several matrices we have defined, but it produces a sequence of covariance estimates having a straightforward interpretation. If we form the matrix $K_P^{(k+1)}$ according to

$$K_P^{(k+1)} = W_P^* \Sigma_P^{(k+1)} W_P ,$$ (47)

then we find that

$$K_P^{(k+1)} = \begin{pmatrix} K_P^{(k+1)}(0) & 0 & 0 & \cdot & \cdot & 0 \\ 0 & K^{(k+1)}(1) & 0 & \cdot & \cdot & 0 \\ \cdot & \cdot & \cdot & \cdot & \cdot & \cdot \\ 0 & 0 & 0 & \cdot & \cdot & K_P^{(k+1)}(I-1) \end{pmatrix},$$ (48)

where $K_P^{(k+1)}(i)$ is a $P{\times}P$ circulant matrix interpreted as the estimate at stage $k{+}1$ of the covariance $K_P(i)$ of the P-periodic reflectance process at delay $m{+}i$. Miller and Snyder [15] show that the (n,m)-element of this circulant matrix is given by

$$\frac{1}{P} \sum_{p=0}^{P-1} E[\, b(p,i) b*(\langle p+n-m \rangle_P, i) \,|\, r , K_P^{(k)} \,],$$ (49)

where $\langle a \rangle_P = a \bmod P$. Equation (49) has an intuitively appealing form. If the reflectivity process $b(n,i)$ could be observed for all instants $n = 0, 1, ..., P-1$ in a period and for each i independently, then the maximum-likelihood estimate of the covariance $K_P(i)$ would be the arithmetic average of the lagged products

$$\frac{1}{P} \sum_{p=0}^{P-1} b(p,i) b*(\langle p+n-m \rangle_P, i).$$ (50)

Equations (48) and (49) indicate that one should simply substitute the conditional mean estimate of an unknown lagged product into this expression to form the maximum-likelihood estimate of the covariance when only the incomplete data are known.

estimating Σ_P and K_P

The maximum-likelihood estimate of Σ_P is a limit point of the sequence defined in (46). The terms on the right side of this equation can be evaluated as follows. Let the conditional-mean estimate of c_P in terms of the incomplete data r be defined at stage k by

$$\hat{c}_P^{(k)} = E[\,c_P | r, \Sigma_P^{(k)}\,]. \tag{51}$$

Then, (46) can be rewritten in the form

$$\Sigma_P^{(k+1)} \overset{d}{=} E[(c_P - \hat{c}_P^{(k)})(c_P - \hat{c}_P^{(k)})^* | r, \Sigma_P^{(k)}] + \hat{c}_P^{(k)}\hat{c}_P^{(k)*}. \tag{52}$$

Now estimating c_P from r, where from (34) and (38)

$$r = \sqrt{2E_T}\,S^*M^*W_P^*c_P + w, \tag{53}$$

is a standard problem in linear estimation-theory. From Tretter [20, Ch. 14], for example, we find that

$$\hat{c}_P^{(k)} = \sqrt{2E_T}\,\Sigma_P^{(k)}W_P MS[2E_T S^*M^*W_P^*\Sigma_P^{(k)}W_P MS + N_0 I]^{-1}r. \tag{54}$$

Furthermore, the first term on the right side in (52) is the covariance of the estimation error when c_P is estimated from r. Also from Tretter [20, Ch. 14], we have

$$\begin{aligned} E[(c_P - \hat{c}_P^{(k)})(c_P - \hat{c}_P^{(k)})^* | r, \Sigma_P^{(k)}] \\ = \Sigma_P^{(k)} - 2E_T \Sigma_P^{(k)}W_P MS[2E_T S^*M^*W_P^*\Sigma_P^{(k)}W_P MS + N_0 I]^{-1}S^*M^*W_P^*\Sigma_P^{(k)}. \end{aligned} \tag{55}$$

In summary, the following steps are performed to produce a sequence $\Sigma_P(0)$, $\Sigma_P(1)$, ..., $\Sigma_P(k)$, ... of estimates of Σ_P for which the corresponding sequence of likelihoods is nondecreasing:

1. set $k = 0$, select a starting estimate $\Sigma_P(0)$;

2. calculate the estimate of c_P according to (54);

3. calculate the error covariance according to (55);

4. update the estimate of Σ_P according to (52);

5. if "last iteration" then stop, else replace k by $k+1$ and go to 2.

The starting value in step 1 can be any positive-definite, diagonal covariance-matrix of dimension $PI \times PI$. Clearly, the processing indicated in (52)-(55) is a nonlinear function of the data.

From (40), a sequence of estimates of K_P having increasing likelihood is obtained from the sequence of estimates of Σ_P according to the following formula:

$$K_P^{(k)} = W_P^* \Sigma_P^{(k)\tau} W_P. \tag{56}$$

estimating the scattering function

Recall that K_P is a block-diagonal matrix with the i-th diagonal block equal to the circulant covariance matrix $K_P(i)$ of the P-periodic reflectance process at delay $m+i$. The first column of this matrix is given by $K_P(i)e$, where e is the P-dimensional unit vector

$$e = \begin{pmatrix} 1 \\ 0 \\ 0 \\ \cdot \\ \cdot \\ 0 \end{pmatrix}. \tag{57}$$

Denote the scattering function of the P-periodic reflectance process at delay $m+i$ by $S(i)$. This is a P-dimensional vector with p-th element given from (14) by

$$S\left(\frac{p}{P}, i\right) = \sum_{n=0}^{P-1} K_P(n,i) \exp\left(-j\frac{2\pi np}{P}\right)$$

$$= \sqrt{P} W K_P(i) e. \tag{58}$$

From this expression, we see that the vector

$$\sqrt{P}\,W_P K_P \begin{pmatrix} e \\ e \\ \cdot \\ \cdot \\ e \end{pmatrix} \qquad (59)$$

is a vector of I vectors of dimension P, the i-*th* of which is the scattering function at delay bin $m+i$. Consequently from (56), a sequence of estimates of the scattering function having increasing likelihood is obtained from the sequence of estimates of Σ_P according to the formula:

$$\sqrt{P}\,\Sigma_P^{(k)} W_P \begin{pmatrix} e \\ e \\ \cdot \\ \cdot \\ e \end{pmatrix}. \qquad (60)$$

Now, the vector

$$\sqrt{P}\,W_P \begin{pmatrix} e \\ e \\ \cdot \\ \cdot \\ e \end{pmatrix}$$

appearing in (60) is an IP-dimensional vector of all ones. As a result, the quantity in (60) is a vector whose elements are the diagonal elements of $\Sigma_P^{(k)}$. Thus, at iteration stage k, the estimate of the scattering function at delay $m+i$ is given by the P diagonal elements of the i-*th* $P{\times}P$ diagonal block of $\Sigma_P^{(k)}$. We may, therefore, simply regard $\Sigma_P^{(k)}$ as the stage k estimate of the scattering function. If the $(p+iI)$-*th* diagonal element of $\Sigma_P^{(k)}$ is the placed in the (p,i) element of a $P{\times}I$-dimensional array, as p varies from 0 to $P-1$ and i varies from 0 to $I-1$, then the result may be displayed as the target's scattering-function image at stage k in range (i coordinate) and cross range (p coordinate).

estimating the reflectance process

It is interesting to note that the k-*th* stage conditional-mean estimate of c_P, given the measurements r and assuming that the second-order statistics of reflectance are given by the k-*th* stage estimate of the scattering function, is used to form the estimate of Σ_P at stage $k+1$ when the expectation-maximization algorithm is used. This estimate is of very much interest in its own right because, from (38), $c_P(i)$ is the Fourier transform of the reflectance process $b_P(i)$. Thus, if the $(p+iI)$-*th* element of this estimate is placed in the (p,i) element of a $P{\times}I$ dimensional array, as p varies from 0 to $P-1$ and i varies from 0 to $I-1$, then the result may be displayed as the target's reflectance image at stage k in range (i coordinate) and cross range (p coordinate).

convergence issues

There are some important properties of the iteration sequence (46) which are worth mentioning. First, each step is in an improving direction. This is shown by writing (52) out as

$$\Sigma_P^{(k+1)} \overset{d}{=} \Sigma_P^{(k)} + \Sigma_P^{(k)} \Theta^{(k)} \Sigma_P^{(k)}, \tag{61}$$

where

$$\Theta^{(k)} = 2E_T W_P M S K_r^{(k)-1} \left(rr^* - 2E_T S^* M^* W_P^* \Sigma_P^{(k)} W_P M S - N_0 I \right) K_r^{(k)-1} S^* M^* W_P^*, \tag{62}$$

and where

$$K_r^{(k)} = 2E_T S^* M^* W_P^* \Sigma_P^{(k)} W_P M S + N_0 I \tag{63}$$

is the k-*th* estimate of the covariance K_r of r. Next, the trace condition (30) which the maximum-likelihood estimate must satisfy is reexamined. From the assumption of the P-periodicity of the reflectance process and the matrix definitions given, the admissible variations δK must be of the form

$$\delta K = M^* W_P^* \delta \Sigma W_P M. \tag{64}$$

Here, $\delta \Sigma$ is a diagonal matrix of the same dimensions as Σ. The trace condition (30) then becomes

$$\mathrm{Tr}\left(K_r^{-1} \left(2E_T S^* M^* W_P^* \Sigma_P W_P M S + N_0 I - rr^* \right) K_r^{-1} S^* M^* W_P^* \delta \Sigma W_P M S \right) = 0. \tag{65}$$

Using the fact that $\mathrm{Tr}(AB) = \mathrm{Tr}(BA)$ and evaluating this trace at the k-*th* iterate, we see that the trace on the left side of (65) is equal to

$$\left(2E_T\right)^{-1}\mathrm{Tr}\left(\Theta^{(k)}\delta\Sigma\right). \tag{66}$$

According to (61), $\Sigma_P^{(k)}$ is changed at each stage by adding the diagonal elements of

$$\Sigma_P^{(k)}\Theta^{(k)}\Sigma_P^{(k)} \tag{67}$$

to $\Sigma_P^{(k)}$. Define

$$\delta\Sigma^{(k)} \stackrel{d}{=} \Sigma_P^{(k)}\Theta^{(k)}\Sigma_P^{(k)}. \tag{68}$$

as these diagonal elements. Then, evaluating the trace at this variation gives

$$\mathrm{Tr}\left(\Theta^{(k)}\delta\Sigma^{(k)}\right) \geq 0. \tag{69}$$

This shows that the variation

$$\delta\Sigma^{(k)}$$

is in an improving direction. Furthermore, we are guaranteed that the incomplete-data loglikelihood is nondecreasing as a result of the M-step of the expectation-maximization algorithm. At this step, the conditional expectation of the complete-data loglikelihood given the incomplete data and the last iterate for Σ_P is maximized over Σ_P. As shown in [15] and [19], this implies that the incomplete-data loglikelihood is nondecreasing.

In the Appendix, we show that if $N_0 > 0$ and the initial guess for Σ_P is positive definite, then each succeeding guess is also positive definite. This gives another interpretation of (69) when $N_0 > 0$. Since the diagonal elements of $\Sigma_P^{(k)}$ are positive, (69) holds with equality if and only if the diagonal elements of $\Theta^{(k)}$ are zero. It follows from this expression (69) that a second property of the sequence (46) is that all stable points of the sequence satisfy the necessary trace condition (30). This is easily shown by noticing that if $\Sigma_P^{(k+1)} = \Sigma_P^{(k)}$, then the diagonal elements (68) are zero. But, this implies that the diagonal elements of $\Theta^{(k)}$ are zero and hence that

$$\mathrm{Tr}\left(\Theta^{(k)}\delta\Sigma\right) = 0 \tag{70}$$

for all diagonal $\delta\Sigma$.

computational considerations

The computations required to produce radar images with our method are specified by (52), (54), (55), and (60) for the scattering-function image and by (52), (54), and (55) for the reflectance image. The number of iterations of these equations that are required to produce an image near the convergence point is presently unknown. Our experience in using an iterative algorithm to produce maximum-likelihood images for emission tomography suggests that 50 to 100 iterations may be necessary, but this is only a guess that will not be verified until some experiments are completed. Some form of specialized processor to accomplish each iteration stage efficiently will probably be needed to produce images in practically useful times. One possible approach is the following. The matrix product

$$\Gamma = \sqrt{2E_T}\,W_r M S$$

is required at each iteration stage and does not change. This $PI{\times}N$-dimensional matrix can, therefore, be computed once off line, stored, and then used as needed during on-line computations. Then, at iteration stage k, the following on-line computations can be performed:

1. compute the $N{\times}N$ matrix A defined by $A = \Gamma^{+}\Sigma_P^{(k)}\Gamma + N_0 I$;

2. compute the $PI{\times}N$ matrix B defined by $B = \Sigma_P^{(k)}\Gamma$;

3. compute $BA^{-1}r$ and the diagonal elements of $\Sigma_P^{(k)} - BA^{-1}B^{+}$.

The computations in 3 can be accomplished in about $4N+PI-2$ time steps using the systolic array described by Comon and Robert [21] augmented, as they suggest, by one row to accomplish the postmultiplication of BA^{-1} by r and by IP rows to accomplish the postmultiplication by B^{+}. The matrix multiplications in 1 and 2 for determining A and B can also be performed rapidly on a systolic array. More study of implementation approaches is needed, but it does not appear that the computational complexity of our new imaging algorithm needs to be a limitation to its practical use.

The choice of N and I is important for the computations. These parameters are selected to achieve a desired range and cross-range resolution and are, therefore, problem dependent, but the same considerations used with other approaches to radar imaging can be used in selecting them. On the other hand, the choice of P is unique to our approach. As stated, we need $P \geq N$, but no upper limit is given. In [18], it is shown that as P increases towards infinity so does the maximum value of the incomplete-data loglikelihood function, with probability one. Thus, P cannot be made arbitrarily large from a theoretical standpoint. Practically, it is desired to have P as small as possible to decrease the memory requirements and the numerical operations. The natural question, then, is what would it mean to have P equal to its smallest allowed value N? For this choice, W is an $N \times N$ matrix and the matrices $K(i)$ are Hermitian symmetric, circulant covariance matrices. Clearly, for a process which is not circulant, this produces an undesirable estimate for K. As P increases, the block diagonal matrices in K_N look less like circulant matrices. Hence, there is a tradeoff involved in the choice of P between the practical constraints of storage and computations and desirable estimates for K. So far as we have been able to determine, there is no theoretical basis for selecting P.

5. Conclusions

The expressions we have obtained for forming images of diffuse, fluctuating radar targets are based on the model stated in Section 2. The target reflectance is assumed to introduce wide-sense-stationary uncorrelated-scattering (WSSUS) of the transmitted signal with no glint or specular components being present. The reflectance process is assumed to be a WSSUS Gaussian process with unknown second-order statistics given by a delay-dependent covariance or scattering function. Echos of the transmitted signal are received from all the reflecting patches that make up the target. Each patch introduces some propagation delay, doppler shift, and random amplitude-scaling into the signal it reflects. The superposition of the echos from all the patches is received in additive noise. Thus, the reflectance process is only observed indirectly following a linear superposition and in additive noise, so neither the reflectance process nor its second-order statistics are known. Target images are made by displaying estimates of either the reflectance process or its second-order statistics (scattering function) based on processing the received signal. In Section 3, we derived the trace condition which the maximum-likelihood estimate of the covariance of the reflectance must satisfy, and we concluded that this condition is too complicated to solve explicitly for the estimate. This motivated the introduction in Section 4 of the incomplete-complete data model and the use of the expectation-maximization algorithm, which results in a sequence of estimates of the scattering function having increasing likelihood. A corresponding sequence of estimates of the reflectance process is also obtained.

There are a number of issues yet to be resolved for the approach we have presented, and we are addressing these. Glint and specular components in the return echos need to be accommodated. The selection of transmitted signals to produce good images is an important subject about which little study has been made. The quality of target images obtained with our new approach is not known at present; to study this issue, we are presently implementing a computer simulation so that comparisons to alternative processing strategies can be made. The equations we have developed are computationally demanding, so special processing architectures will be important to make their use practical.

6. References

1.   M. J. Prickett and C. C. Chen, "Principles of Inverse Synthetic Aperture Radar (ISAR) Imaging," IEEE EASCON Record, pp. 340-345, September 1980.

2.   K. Ruttenberg and L. Chanzit, "High Range Resolution by Means of Pulse to Pulse Frequency Shifting," IEEE EASCON Record, 1968.

3.   C.-C. Chen and H. C. Andrews, "Multifrequency Imaging of Radar Turntable Data," IEEE Trans. on Aerospace and Electronic Systems, Vol. AES-16, pp. 15-22, January 1980.

4.   D. L. Mensa, *High-Resolution Radar Imaging*, Artech House, Dedham, Mass., 1984.

5.   J. L. Walker, "Range-Doppler Imaging of Rotating Objects," IEEE Transactions on Aerospace and Electronic Systems, Vol. AES-16, No. 1, pp. 23-52, January 1980.

6.   D. C. Munson, Jr., J. D. O'Brian, and W. K. Jenkins, "A Tomographic Formulation of Spotlight-Mode Synthetic Aperture Radar," Proceedings of the IEEE, Vol. 71, pp. 917-925, August 1983.

7.   R. E. Blahut, "Segmented-Chirp-Waveform Implemented Radar-System," U. S. Patent No. 4309703, January 1982.

8.   M. Bernfeld, "CHIRP Doppler Radar," Proceedings of the IEEE, Vol. 72, pp. 540-541, April 1984.

9.   D. L. Snyder, H. J. Whitehouse, J. T. Wohlschlaeger, and R. Lewis, "A New Approach to Radar/Sonar Imaging," Proc. SPIE Conference on Advanced Algorithms and Architectures, Vol. 696, San Diego, CA, August 1986.

10. D. L. Snyder, L. J. Thomas, Jr., and M. M. Ter-Pogossian, "A Mathematical Model for Positron Emission Tomography Systems Having Time-of-Flight Measurements," IEEE Transactions on Nuclear Science, Vol. NS-28, pp. 3575-3583, June 1981.

11. D. L. Snyder and D. G. Politte, "Image Reconstruction from List-Mode Data in an Emission Tomography System Having Time-of-Flight Measurements," IEEE Transactions on Nuclear Science, Vol. NS-30, pp. 1843-1849, 1983.

12. H. L. Van Trees, *Estimation, Detection, and Modulation Theory, Vol. 3*, John Wiley and Sons.

13. J. Shapiro, B. A. Capron, and R. C. Harney, "Imaging and Target Detection with a Hetrodyne-Reception Optical Radar, Applied Optics, Vol. 20, No. 19, pp. 3292-3313, October 1981.

14. V. S. Frost, J. A. Stiles, K. S. Shanmugan, and J. C. Holtzman, "A Model for Radar Images and Its Application to Adaptive Digital Filtering of Multiplicative Noise," IEEE Transactions on Pattern Analysis and Machine Intelligence, Vol. PAMI-4, No. 2, pp. 643-652, March 1982.

15. M. I. Miller and D. L. Snyder, "The Role of Likelihood and Entropy in Incomplete-Data Problems: Applications to Estimating Point-Process Intensities and Toeplitz-Constrained Covariances," Proceedings of the IEEE, Vol. 75, No. 7, July 1987.

16. M. Turmon and M. I. Miller, "Performance Evaluation of Maximum-Likelihood Estimates of Toeplitz Convariances Generated with the Expectation-Maximization Algorithm," 1987 Conference on Information Sciences and Systems, Johns Hopkins University, Baltimore, MD, pp. 25-27, 1987.

17. J. P. Burg, D. G. Luenberger, and D. L. Wenger, "Estimation of Structured Covariance Matrices," Proc. IEEE, Vol. 70, No. 9, pp. 963-974, September 1982.

18. D. R. Fuhrmann and M. I. Miller, "On the Existence of Positive Definite Maximum-Likelihood Estimates of Structured Covariance Matrices," IEEE Transactions on Information Theory, in review.

19. A. D. Dempster, N. M. Laird, and D. B. Rubin, "Maximum Likelihood from Incomplete Data Via the EM Algorithm," J. of the Royal Statistical Society, Vol. B, 39, pp. 1-37, 1977.

20. S. A. Tretter, *Introduction to Discrete-Time Signal Processing*, John Wiley and Sons, New York, 1976.

21 P. Comon and Y. Robert, "A Systolic Array for Computing BA^{-1}," IEEE Trans. on Acoustics, Speech and Signal Processing, Vol. ASSP-35, No. 6, pp. 717-723, June 1987.

7. Appendix

derivation of the trace condition (30)

From the definition of the loglikelihood function in (28), we have

$$\frac{1}{\alpha}\left(L_{id}(K+\alpha\delta K)-L_{id}(K)\right)$$

$$=-\frac{1}{2\alpha}r^{\ast}\left((K_r+\alpha 2E_T S^{\ast}\delta KS)^{-1}-K_r^{-1}\right)r-\frac{1}{2\alpha}\ln\left(\det(K_r+\alpha 2E_T S^{\ast}\delta KS)\det(K_r^{-1})\right),$$

(A1)

where K_r is the covariance of the incomplete data r as given in (26). Examining the first term on the right, we have that it equals

$$-\frac{1}{2\alpha}r^{\ast}K_r^{-1}\left(\left(I+\alpha 2E_T S^{\ast}\delta KSK_r^{-1}\right)^{-1}-I\right)r$$

$$=\frac{1}{2\alpha}r^{\ast}K_r^{-1}\left(\alpha 2E_T S^{\ast}\delta KSK_r^{-1}\right)\left(I+\alpha 2E_T S^{\ast}\delta KSK_r^{-1}\right)^{-1}r$$

$$=\frac{1}{2}r^{\ast}K_r^{-1}2E_T S^{\ast}\delta KSK_r^{-1}r+O(\alpha).$$

(A2)

Examining the second term on the right in (A1), we have

$$-\frac{1}{2\alpha}\ln\left(\det\left(I+\alpha 2E_T S^{\ast}\delta KSK_r^{-1}\right)\right)=-\frac{1}{2\alpha}\ln(\det(I+\alpha B))$$

$$=-\frac{1}{2\alpha}\ln\left(1+\alpha\operatorname{Tr}(B)+\ldots+\alpha^{n}\det(B)\right)$$

$$=-\frac{1}{2}\operatorname{Tr}(B)+O(\alpha),$$

(A3)

where B is defined in the first equality. Equations (A2) and (A3) imply that

$$r^{\ast}K_r^{-1}2E_T S^{\ast}\delta KSK_r^{-1}r-\operatorname{Tr}\left(2E_T S^{\ast}\delta KSK_r^{-1}\right)=0,$$

(A4)

which is the trace condition (30).

derivation of the sign-definiteness condition

To check the sign-definiteness of the second derivative of the loglikelihood $L_{id}(K)$, we form the limit

$$\lim_{\alpha \to 0} \frac{1}{|\alpha|} \mathrm{Tr}\big(\big(2E_T S^*(K+\alpha\delta K)S + N_0 I \big)^{-1} \big(rr^* - N_0 I - 2E_T S^*(K+\alpha\delta K)S \big)$$

$$\times \big(2E_T S^* KS + \alpha 2E_T S^* \delta KS + N_0 I \big)^{-1} S^* \delta KS$$

$$- K_r^{-1} \big(rr^* - N_0 I - 2E_T S^* KS \big) K_r^{-1} S^* \delta KS \big)$$

$$= \mathrm{Tr}\big(K_r^{-1} 2E_T S^* \delta KS K_r^{-1} \big(2E_T S^* KS + N_0 I - 2rr^* \big) K_r^{-1} 2E_T S^* \delta KS \big).$$

(A5)

A necessary condition for K to be a relative maximum is that this last expression evaluated at K be equal to or less than zero for all admissible variations δK. Under the assumptions in Section 4, admissible variations are given by (64). Substituting (64) into (A5) and evaluating for all diagonal matrices $\delta\Sigma$ gives the second-order necessary condition. A sufficient condition for K to be a strict local maximum is that the trace condition (30) is satisfied and that (A5) is strictly negative for all admissible variations.

estimating a general Toeplitz matrix

In Section 4, we derived a sequence of estimates for a covariance matrix subject to the constraint that the estimates must be circulant Toeplitz matrices. For completeness, we develop and discuss in this section the equations for estimating a covariance matrix subject to the weaker constraint that the estimates be general Toeplitz matrices. Similar equations for other constraints on the Toeplitz matrices are easily obtained by mimicking the steps in the main body of this paper.

Let the complete data be $\{b, w\}$, and let b be normally distributed with zero mean and covariance K, as given in (27). The complete-data loglikelihood is given in (35). Maximizing this function gives the trace condition

$$\mathrm{Tr}\big(K^{-1}(bb^* - K)K^{-1}\delta K \big) = 0,$$

(A6)

which the maximum-likelihood estimate K must satisfy. Performing the E and M steps of the expectation-maximization algorithm yields the following iteration sequence for the elements $K(n,i)$, $n = 0, 1, ..., N-1$, of the covariance matrix $K(i)$ defined in (25):

$$K^{(k+1)}(n,i) = \frac{1}{N-n} \mathrm{E}\big[\sum_{j=0}^{N-n-1} b(j, m+i)b^*(j+n, m+i) \,|\, r, K^{(k)} \big].$$

(A7)

In matrix form,

$$K^{(k+1)} = K^{(k)} + 2E_T K^{(k)} S K_r^{(k)-1} \left(r r^* - 2 E_T S^* K^{(k)} S - N_0 I \right) K_r^{(k)-1} S^* K^{(k)}, \tag{A8}$$

where

$$K_r^{(k)} = 2 E_T S^* K^{(k)} S + N_0 I. \tag{A9}$$

If this iteration converges to a stable point, then the trace condition is satisfied at that point, as may be shown by using the same arguments as in Section 4. It is worth restating that the reason this iteration is not recommended here is that the probability that the iteration sequence generates a singular estimate for K approaches one as N gets large. By restricting consideration to Toeplitz matrices with circulant extensions, the loglikelihood function is bounded with probability one for finite extensions and a positive definite K is generated with probability one, as proven by Fuhrmann and Miller [18].

proof that $\Sigma_P(k)$ is positive definite for every k

Assume that the initial guess $\Sigma_P(0)$ for Σ_P is positive definite and that $N_0 > 0$. We will now show that if $\Sigma_P(k)$ is positive definite, then so is $\Sigma_P(k+1)$, and thus, by induction, $\Sigma_P(k)$ is positive definite for all k. One key to following this derivation is the matrix identity

$$B(I + AB)^{-1} = (I + BA)^{-1} B. \tag{A10}$$

This identity is used to rewrite (62) as

$$\begin{aligned}
\Sigma_P^{(k+1)} \overset{d}{=} \; & H(N_0 2 E_T \Sigma_P^{(k)} W_P M S S^* M^* W_P^* \Sigma_P^{(k)} + N_0^2 \Sigma_P^{(k)} \\
& + 2 E_T \Sigma_P^{(k)} W_P M S r r^* S^* M^* W_P^* \Sigma_P^{(k)}) H^* \\
= \; & N_0 2 E_T \left(H \Sigma_P^{(k)} W_P M S \right) \left(S^* M^* W_P^* \Sigma_P^{(k)} H^* \right) \\
& + 2 E_T \left(H \Sigma_P^{(k)} W_P M S r \right) \left(r^* S^* M^* W_P^* \Sigma_P^{(k)} H^* \right) \\
& + N_0^2 H \Sigma_P^{(k)} H^*,
\end{aligned} \tag{A11}$$

where we have defined H according to

$$H = \left(2 E_T \Sigma_P^{(k)} W_P M S S^* M^* W_P^* + N_0 I \right)^{-1}. \tag{A12}$$

Clearly, all the diagonal elements of (A11) are greater than or equal to zero. To show that they are strictly positive, we look at the last term and get that the i-*th* diagonal element is

$$\left(N_0^2 H \Sigma_P^{(k)} H^* \right)_{ii} = N_0^2 \sum_{j=0}^{I_P-1} (H)_{ij} \left(\Sigma_P^{(k)} \right)_{jj} (H^*)_{ji}$$

$$= N_0^2 \sum_{j=0}^{I_P-1} |(H)_{ij}|^2 \left(\Sigma_P^{(k)} \right)_{jj}, \qquad (A13)$$

which is clearly positive when $N_0 > 0$ since H is invertible and all diagonal elements of $\Sigma_P(k)$ are positive.

END

10-87

DTIC